# Advanced flame-retardant biocomposites: Polylactic acid reinforced with green gallic acidironphosphorus coated flax fibers

International Journal of Biological Macromolecules 300 (2025) 140215

Contents lists available at ScienceDirect

International Journal of Biological Macromolecules

journal homepage: www.elsevier.com/locate/ijbiomac

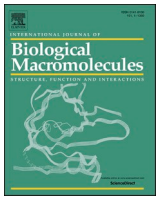

# Advanced flame-retardant biocomposites: Polylactic acid reinforced with green gallic acid-iron-phosphorus coated flax fibers

Alessia Pantaleoni [a,*], Assunta Marrocchi [b], Pietro Russo [c], Giulio Malucelli [d], Davide Altamura [e], Francesca Nardelli [f,g], Silvia Pizzanelli [f,h], Angelo Freni [f], Cinzia Giannini [e], Maria Laura Santarelli [a], Irene Bavasso [a], Maria Paola Bracciale [a], Fabrizio Sarasini [a]

[a] Department of Chemical Engineering Materials Environment, Sapienza University of Rome, Via Eudossiana 18, 00184 Rome, Italy
[b] Department of Chemistry, Biology and Biotechnology, University of Perugia, Via Elce di Sotto 8, 06123 Perugia, Italy
[c] Institute for Polymers, Composites and Biomaterials, National Research Council, Via Campi Flegrei 34, 80078 Pozzuoli, Na, Italy
[d] Department of Applied Science and Technology, Politecnico di Torino, Viale Teresa Michel 5, 15121 Alessandria, Italy
[e] Institute of Crystallography, National Research Council, v. Amendola 122/O, 70126 Bari, Italy
[f] Institute for the Chemistry of OrganoMetallic Compounds, Italian National Research Council, CNR-ICCOM, Via Giuseppe Moruzzi 1, 56124 Pisa, Italy
[g] Department of Chemistry and Industrial Chemistry, University of Pisa, Via Giuseppe Moruzzi 13, 56124 Pisa, Italy
[h] Centre for Instrument Sharing (CISUP), University of Pisa, Lungarno Pacinotti 43, 56126 Pisa, Italy

ARTICLE INFO

*Keywords:*
Biocomposites
Gallic acid-hybrid flame retardants
Coating
Flax fiber
Polylactic acid (PLA)
Smoke suppression

ABSTRACT

This study introduces a sustainable approach for enhancing the fire retardancy and smoke suppression of poly (lactic acid) (PLA) composites, contributing to addressing one of the major challenges in biocomposites that limits their application in various engineering fields, as automotive and construction sectors. Flax fibers (FF) were surface functionalized with a novel organic-inorganic hybrid flame retardant (FR), offering a sustainable bioinspired approach that mitigates potential mechanical properties impairment and FR leaching, which can cause environmental concerns and reduced composite durability.

The process involves a three-step coating procedure. First, the flax fibers (FF) are pretreated with ozone to promote carboxylic group formation (FF-$O_3$); subsequently, gallic acid (GA) units are covalently immobilized on the fiber surface (FF-GA); finally, the hybrid FR iron phenylphosphonate is complexed with the phenolic groups of GA units (FF-GA-FeP).

Fourier transform infrared (FT-IR) analysis of FF-GA-FeP confirmed the presence of specific absorptions associated with the deposited FR coating. Scanning electron microscopy coupled with energy-dispersive X-ray spectroscopy (SEM-EDS) revealed changes in fiber morphology and confirmed the incorporation of iron and phosphorus. Solid-state nuclear magnetic resonance (SSNMR) spectroscopy and X-ray WAXS microscopy revealed that fibers' crystallinity was not significantly affected by derivatization. Microwave plasma atomic emission spectroscopy (MP-AES) detected a precise 0.1 wt% iron loading.

Using FF-GA-FeP as reinforcement in PLA-based composites (PLA/FF-FeP) resulted in enhanced thermal stability and flame retardancy of the composites, with minimal coating application, as revealed by thermogravimetric analysis (TGA) and cone calorimetry tests (CCT). A decrease in peak of heat release rate (pHRR), total smoke release (TSR), specific extinction area (SEA), and Fire Propagating Index (FPI) of 5, 87, 68, and 9.5 %, respectively, was achieved for PLA/FF-FeP, compared to untreated flax fiber reinforced PLA (PLA/FF). Furthermore, preliminary tensile tests indicate minor changes in tensile strength and a slight increase in stiffness of the PLA/FF-FeP compared to PLA/FF.

Hence, in the biocomposite, the immobilization of a minimal amount of iron phenylphosphonate directly on the flax fiber surface proved to be an effective strategy for smoke suppression while preserving the mechanical integrity of the composite.

* Corresponding author.
*E-mail address:* alessia.pantaleoni@uniroma1.it (A. Pantaleoni).

https://doi.org/10.1016/j.ijbiomac.2025.140215
Received 21 October 2024; Received in revised form 30 December 2024; Accepted 20 January 2025
Available online 22 January 2025

## 1. Introduction

Fiber reinforced polymer composites (FRPs) have been widely adopted by such industries as automotive, construction, aerospace, and marine [1] due to their distinctive specific mechanical properties. However, growing environmental concerns regarding non-renewable sourced materials, coupled with stringent environmental regulations [2] have driven research toward the development of alternative high-performance biobased materials. In this context, biopolymers reinforced with natural fibers have emerged as promising sustainable alternatives to traditional polymer composites reinforced with synthetic fibers [3]. Polylactic acid (PLA), derived from renewable feedstock [4], has received considerable attention for its versatility in applications ranging from packaging to fiber production and composite manufacturing [5]. Several studies have explored the properties of PLA reinforced with different types of lignocellulosic fibers, such as hemp [6], flax [7], ramie [8], and bamboo [9]. The interesting physical and specific mechanical properties, coupled with their low production costs and sustainable environmental characteristics, make them attractive for application as non-structural components in the transportation sector [10].

However, challenges persist in such composites, notably the poor adhesion between the hydrophilic natural fiber and the hydrophobic polymer matrix. [11] This issue has been extensively studied, and different solutions have been proposed [12], including finishing treatments of the natural fibers with ionic liquids [13] or silane coupling agents [14].

In addition, these composites are prone to burn easily. Such biopolymers as PLA are inherently highly flammable, exacerbating fire spread due to extensive dripping phenomena [15]. The presence of the natural fibers further reduces the fire resistance compared to synthetic reinforcing fibers like glass fibers [16]. Moreover, the combustion of these materials not only accelerates flame propagation but also generates significant amounts of smoke and toxic gases, which impair visibility and pose serious health risks [17]. These hazards, including the release of irritant compounds and asphyxiating gases like carbon monoxide, make escape and rescue operations more difficult and increase the danger for trapped individuals [18]. To mitigate these risks, the prevailing strategy involves the direct incorporation of flame retardants (FRs) into the polymer matrix [19].

Based on their structure, FRs can be classified into organic, inorganic, and organic-inorganic hybrids. Hybrid organic-inorganic flame retardants combine the advantages of both inorganic and organic materials [20]. In particular, the inorganic element, due to its incombustible nature and high specific heat capacity, enhances the composite's overall thermal stability and fire safety by releasing water vapor and/or providing a physical barrier toward heat and mass transfer, thereby reducing the intensity and propagation of flames [21,22]. The organic component, alongside enhancing the flame retardant efficiency [23], fosters compatibility with the polymer matrix, which, on the other hand, is extremely reduced in the case of inorganic FRs [24]. This ensures an effective dispersion of the flame retardant without compromising the mechanical properties of the polymer [25]. In this context, iron phosphonate is an example of hybrid FR where the concurrence of radical scavenging effects in the gas phase by the organic component and catalytic charring in the condensed phase by the inorganic component occurs [26,27].

However, adding FRs directly in the polymer matrix has an inherent risk of FR leaching out of the matrix [28], thus contaminating the environment [29] and reducing the overall composite performance. Moreover, when a polymer is reinforced with cellulosic fibers, it is susceptible to the “candlewick effect” [30] due to the higher thermal conductivity of the fibers. One of the most widely used commercial phosphorus-based flame retardants (FRs) is ammonium polyphosphate (APP) [31]. Shumao et al. [32] studied ramie fiber-reinforced PLA composites with APP applied in three different configurations: blended into the PLA matrix, applied to the fibers, and a combination of both. They found that treating the fibers with APP rather than incorporating it directly into the matrix preserved the mechanical properties. In addition, besides to circumventing potential leaching of the flame retardant (FR), which might occur when FR is directly dispersed within the polymer matrix [33], this approach effectively mitigated the “candlewick effect”, enhancing fire safety by promoting char formation and reducing flame spread. Liu et al. [34] and Chen et al. [35] demonstrated that grafting 9,10-Dihydro-9-oxa-10-phosphaphenanthrene-10-oxide (DOPO), a commercial flame retardant, directly onto the surface of glass fibers and incorporating the latter as reinforcement in epoxy resin or polyamide 6-based composites resulted in improved fiber-matrix adhesion, circumvented FR leaching, and enhanced the fire behavior of composites. These findings reinforce the effectiveness of applying flame retardants directly to fibers, rather than dispersing them within the polymer matrix, as it limits mechanical degradation while providing excellent flame-retardant performance.

This study builds upon such advancements by introducing a bio-inspired protocol for coating flax fiber (FF) with a low loading of halogen-free hybrid FR to increase the fire retardancy and suppress smoke production of PLA-based biocomposites. The hybrid FR, i.e., iron phenylphosphonate (FeP) complex, was immobilized on the FF surface to achieve a good dispersion within the matrix and to provide the previously mentioned benefits, such as fiber protection in case of fire by favoring char production, limitation of the “candlewick effect”, and promotion of radical scavenging reactions in the gas-phase. This work, to preserve the environmentally friendly character of the biocomposites, proposes, for the first time, a biobased and bioinspired process for FR covalent immobilization on fiber surface. The protocol involves the covalent immobilization of renewable gallic acid units, a phenolic acid of biological origin widely found in waste vegetable biomass [36], that allow the in-situ complexation of iron phenylphosphonate to form the hybrid FR-coated fiber. Inspired by the siderophore enterobactin's iron acquisition mechanism [37], this process mimics nature's efficiency in coordinating $Fe^{III}$ through catecholate groups, given the gallic acid structural similarity to the iron coordinating moiety in bacteria. Different studies are reported in the literature to increase the fire resistance of composites by incorporating iron phosphonate FRs into the matrix [38–40], but approaches of immobilizing the hybrid FR on the fiber surface are limited. For instance, Zhang et al. [41] proposed a pre-deposition of polymerized polydopamine on the flax fiber surface to graft the hybrid FR, which differs from the covalent bonding proposed in this work. While their method achieved improved flame resistance, it required a significantly higher FR loading (6.1 wt%) compared to the minimal amount used in our system.

To complete the investigation, extensive characterization validates the effectiveness of the designed functionalization protocol, with Fourier-transform infrared (FT-IR) spectroscopy, scanning electron microscopy coupled with energy dispersive X-ray spectroscopy (SEM-EDS), microwave plasma atomic emission spectroscopy (MP-AES), thermogravimetric analysis (TGA), solid-state nuclear magnetic resonance (SSNMR) spectroscopy and Small/Wide-Angle X-Ray Scattering (SAXS/WAXS), confirming successful FR-FF coating without a significant reduction in the crystallinity of the fibers. The FR-coated fibers were then used as reinforcement in PLA-based composites (PLA/FF-FeP), the fire behavior of which was assessed by cone calorimetry tests (CCT); further, the mechanical behavior of the flame retarded composites was investigated through tensile tests.

## 2. Materials and methods

### 2.1. Materials

Flax fibers were provided by Teillage Vandecandelaere (Bourguebus, France) with a nominal length of 2 mm and without any specific sizing treatment. Flax fabric was provided by Composites Evolution (UK) as a

2 × 2 twill Biotex fabric with an areal weight of 200 g/m$^2$. A PLA Luminy® LX175 (96 % (L-isomer)) supplied by TotalEnergies Corbion was used as polymer matrix. Gallic acid (GA, $C_7H_6O_5$) was purchased from Thermo Scientific™. Thionyl chloride ($SOCl_2$), tert-amyl methyl ether (TAME), iron (III) chloride hexahydrate ($FeCl_3{\cdot}6H_2O$), and phenylphosphonic acid (PPA, $C_6H_5P(O)(OH)_2$) were obtained from Merck KGaA, Darmstadt, Germany, and used without further purification unless otherwise stated.

### 2.2. Methods

#### 2.2.1. Flax fiber ozonization process

A Salinovo ozone generator was utilized to pretreat flax fibers and fabrics with ozone ($O_3$). This generator operated on an air-feed system and reached a maximum diffusion rate of 0.5 h$^{-1}$. A total of 20 g of flax fibers were placed in a 500 cm$^3$ ozonation chamber, where ozone was introduced through a porous diffusion plate. The treatment was conducted for up to 7 h.

#### 2.2.2. Galloyl chloride synthesis

Gallic acid (34 g, 0.2 mol) and thionyl chloride (100 mL, 0.9 mol) were combined in a single-neck flask. The reaction mixture was heated to 80 °C for 3 h. Once the reaction time had elapsed, the excess thionyl chloride was removed under vacuum. The resulting crude galloyl chloride was used in the subsequent reaction without any further purification.

FT-IR (cm$^{-1}$): 2800–3400 (O—H stretching); 1747 (C═O stretching), 732, 692, 632, 589 (C—Cl stretching) [42].

#### 2.2.3. Flax fiber coating

The crude galloyl chloride (36.9 g) was dissolved in TAME (270.6 g, 2.6 mol) to reach a 12 % (w/w) solution. 30 g of flax fibers were immersed in this solution and stirred for 2 h. Afterward, the mixture was washed with deionized water and dried in a ventilated oven at 80 °C for 2 h.

Subsequently, 36 g of flax fibers functionalized with gallic acid units (FF-GA) were placed in a beaker containing 520 mL of deionized water. To this, 130 mL of an aqueous solution of $FeCl_3{\cdot}6H_2O$ (0.82 g, 3 mmol) was added. The mixture was stirred, and after 6 h, PPA (0.96 g, 6 mmol), which had been dissolved in 130 mL of deionized water, was added dropwise. The reaction was conducted at room temperature for 12 h. Finally, the iron phosphonate-coated flax fibers (FF-GA-FeP) were washed with deionized water and dried overnight in a ventilated oven at 85 °C.

#### 2.2.4. Composite manufacturing

PLA/FF, PLA/FF-$O_3$, and PLA/FF-FeP composites were fabricated using a Brabender-like apparatus (Rheocord EC, Haake Inc.) and a lab-scale hydraulic press (Collin model P400E) to create plates with dimensions of 100 mm × 100 mm × 4 mm. Before compounding, the flax fibers (FF, FF-$O_3$, FF-GA-FeP) and PLA pellets were subjected to drying in a vacuum oven at 70 °C for 4 h. The micro compounder was employed to mix FF, FF-O3, and FF-GA-FeP with PLA at a rotational speed of 60 rpm and a temperature of 180 °C for 5 min. Subsequently, the PLA composites were compression-molded at 180 °C following this pressure sequence: 2 min at 0 bar, 1 min at 5 bar, 1 min at 10 bar, and 1 min at 20 bar. The cooling step was carried out until reaching room temperature while keeping the material at a maximum pressure of 20 bar. The fiber content was maintained at 20 wt%.

For the tensile testing, the composites were prepared through an injection molding technique (Haake MiniJet II Pro, Thermo Fisher Scientific). During the injection process, the loading cylinder temperature was set to 190 °C, whereas the mold temperature was held at 45 °C.

All details about characterization techniques are reported in the supporting information.

## 3. Results and discussion

### 3.1. Preparation and characterization of flax fiber coating

The hybrid FR-FF coating protocol involved three main steps: (I) oxidation of the cellulosic component of FF via $O_3$ pretreatment (FF-$O_3$); (II) covalent immobilization of gallic acid (GA) units by anhydride bond formation (FF-GA); (III) promotion of the in-situ complexation of iron phenylphosphonate (FeP) by phenolic groups of the immobilized GA units (FF-GA-FeP), resulting in the hybrid FR-coated fiber, as depicted in Fig. 1.

Previous literature described oxidation processes of cellulose microfibrils [43] and flax fibers [44] using 2,2,6,6-tetramethylpiperidine-1-oxyl (TEMPO) to create surface carboxyl groups. However, TEMPO is associated with challenges including high corrosiveness, difficult handling [45], and environmental toxicity, particularly concerning its impact on the biosphere [46]. In this work, ozone ($O_3$) is proposed as a safer oxidizing agent [47], able to convert the primary surface hydroxyl groups of the cellulosic component (which is approximately 70 % of the total fiber) [48] into carboxyl groups [49].

Fig. 2 presents the FT-IR spectra of untreated (FF) and pretreated FF with $O_3$ (FF-$O_3$). The untreated fiber spectrum shows signals associated with hemicellulose and cellulose [50], which are the main components of FF (Table 1). A new absorption at 1731 cm$^{-1}$ ascribed to carboxyl group (C═O) is observed in the FF-$O_3$ spectrum [43–45], validating the ozone effectiveness in the cellulose hydroxyl group oxidation to carboxyl group.

The effect of the ozonation process on FF was further evaluated by SEM and thermogravimetric analyses. The micrographs shown in Fig. S1 reveal no significant differences in morphology between FF and FF-$O_3$.

Thermogravimetric results of untreated FF and FF-$O_3$, depicted in Fig. 3, highlight that the untreated FF experiences a maximum decomposition rate temperature ($T_{max}$) at 358 °C [51], and a residual weight at 800 °C of 17 %. FF-$O_3$ exhibits a slight reduction in the maximum degradation temperature (354 °C) and an increase in the residual weight (27 %). This is attributed to the high reactivity of ozone with phenolic and polyphenolic structures, which in flax fiber results in partial removal of lignin [52], Consequently, the reduction in lignin content accounts for a lower $T_{max}$ and a higher percentage of thermally non-degradable elements, increasing the residual weight in FF-$O_3$ [47].

In the second step (II) of the coating protocol, the carboxyl groups of FF-$O_3$ were used to immobilize the designed FR complex, as depicted in Fig. 1.

Galloyl chloride was obtained via a solvent-free method, following established procedures [53]. Subsequently, a 12 % (w/w) mixture of galloyl chloride was prepared in green tert-amyl methyl ether [54,55]. The reaction between the carboxyl groups of FF-$O_3$ and the acyl group of galloyl chloride enabled the immobilization of gallic acid units on the fiber surface via anhydride bond formation. The resulting fiber functionalized with GA units was named FF-GA.

Fig. 4 compares the FT-IR spectra of FF-GA and FF-$O_3$. In the FF-GA spectrum, signals that can be associated with fiber-bound gallic acid units are observed: the absorption at 3493 cm$^{-1}$ is due to O—H stretching of the phenolic ring, while absorptions at 1609 cm$^{-1}$ and 1540 cm$^{-1}$ are due to C═C stretching of the aromatic ring [56]. The signals at 1264 cm$^{-1}$, 1219 cm$^{-1}$ and 767 cm$^{-1}$ are attributed to C—O stretching, O—H bending and C—C stretching respectively, while the absorptions at 866 cm$^{-1}$, 799 cm$^{-1}$, and 733 cm$^{-1}$ are ascribed to C—H bending [57].

The success of the second step was further confirmed by a morphological modification of the FF surface, as highlighted by SEM micrographs (Fig. 5). In Fig. 5b, the clean and smooth surface of the untreated fiber (Fig. 5a) is replaced by the appearance of a new rough coating on the fiber surface, resulting from the immobilization of GA.

In the third coating step (III), inspired by the iron acquisition bacterial process, iron phenylphosphonate was complexed to the phenolic

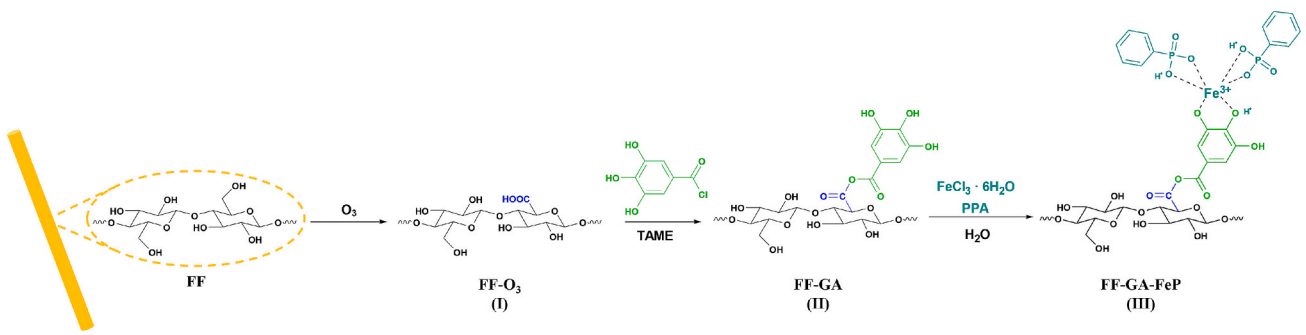


**Fig. 1.** Reaction pathway for FF surface modification.

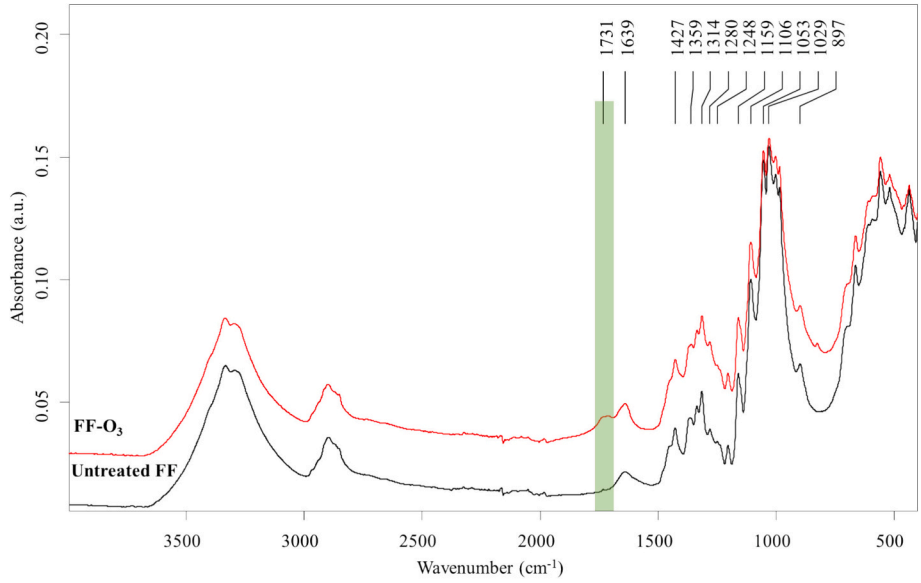


**Fig. 2.** Infrared spectra of untreated FF (black line) and FF-$O_3$ (red line).

**Table 1**
Infrared assignments of FF.

| Wavenumber ($cm^{-1}$) | Functional group[a] |
|---|---|
| 3700–3000 | νOH Intra- and intermolecular of cellulose |
| 2990–2754 | νCH of cellulose and hemicellulose |
| 1639 | δHOH of water in crystalline cellulose |
| 1427, 1359, 1314 | $\delta CH_2$, δCH of cellulose and $\omega CH_2$ of cellulose and hemicellulose |
| 1280 | $\tau C\text{-}H_2$ of cellulose |
| 1248, 1159, 1106, 1029 | νC—O—C e νC—C of polysaccharide compounds (mainly cellulose) |
| 1053 | νC—OH of cellulose and hemicellulose |
| 897 | β-glycosidic bonds between the glucose units of cellulose |

[a] $\nu$ = stretching; $\delta$ = bending; $\omega$ = wagging; $\tau$ = twisting.

groups of the GA units previously immobilized on the FF surface (Fig. 1) [58]. The reaction between FF-GA and $FeCl_3{\cdot}6H_2O$ took place in water at room temperature. Under these conditions, the dissociation of ferric chloride provides the metal ions required for complexation with phenolic groups, while the release of hydrochloric acid (HCl) contributes to acidifying the reaction environment. At pH < 5, the formation of iron(III) mono(catecholate) complexes was ensured [59]. For the synthesis of iron phenylphosphonate, phenylphosphonic acid (PPA) was added to the reaction system. The high affinity of phosphonate moiety oxygen atoms to $Fe^{III}$ [60] allowed for tight binding of iron phosphonate to gallic acid units immobilized on the FF surface, resulting in the formation of FR-coated flax fibers (FF-GA-FeP).

FF-GA-FeP was characterized by SEM-EDS analysis, as shown in Fig. 6. The typical micrographs show the presence of a new globular coating on the fiber surface, while EDS analysis reveals the presence of Fe and P, which can be attributed to the deposition of the iron phenylphosphonate coating.

The MP-AES analysis on FF-GA-FeP detected a very low iron loading (namely, 0.1 wt%), which, nevertheless, confirms the $Fe^{III}$-gallic acid units complexation on FF surface.

Untreated FF, FF-GA, and FF-GA-FeP were analyzed by thermogravimetric analysis. TG and DTG curves are reported in Fig. 7, while Table S1 summarizes the onset degradation temperatures at a weight loss of 5 % ($T_{5\%}$) and 10 % ($T_{10\%}$), the temperature at the maximum decomposition rate ($T_{max}$), and the final residue at 800 °C.

The fiber functionalized with GA units exhibited a maximum decomposition rate temperature ($T_{max}$) at 333 °C, lower than untreated FF (358 °C). This decrease is due to the presence of gallic acid units [61] on the fiber surface, which exhibited a $T_{max}$ of 265 °C (Fig. S2), i.e., anticipating the degradation of the fiber due to the acidic functionalization. Additionally, the presence of GA affects the residual weight of FF-GA (about 10.8 %), which is lower than the untreated fiber (16.8 %), due to the thermal degradation of GA units bound to the fiber surface, which exhibited a residual weight of 1 % at 800 °C (Fig. S2). FF-GA-FeP showed a $T_{max}$ at 341 °C, marginally higher compared to the $T_{max}$ of FF-GA. This slight enhancement in fiber thermal stability is attributed to the incorporation of FeP, which has a $T_{max}$ of 479 °C as evaluated by thermogravimetric analysis of the as-synthesized complex (Fig. S3). Furthermore, FF-GA-FeP showed a modest increase in residual weight

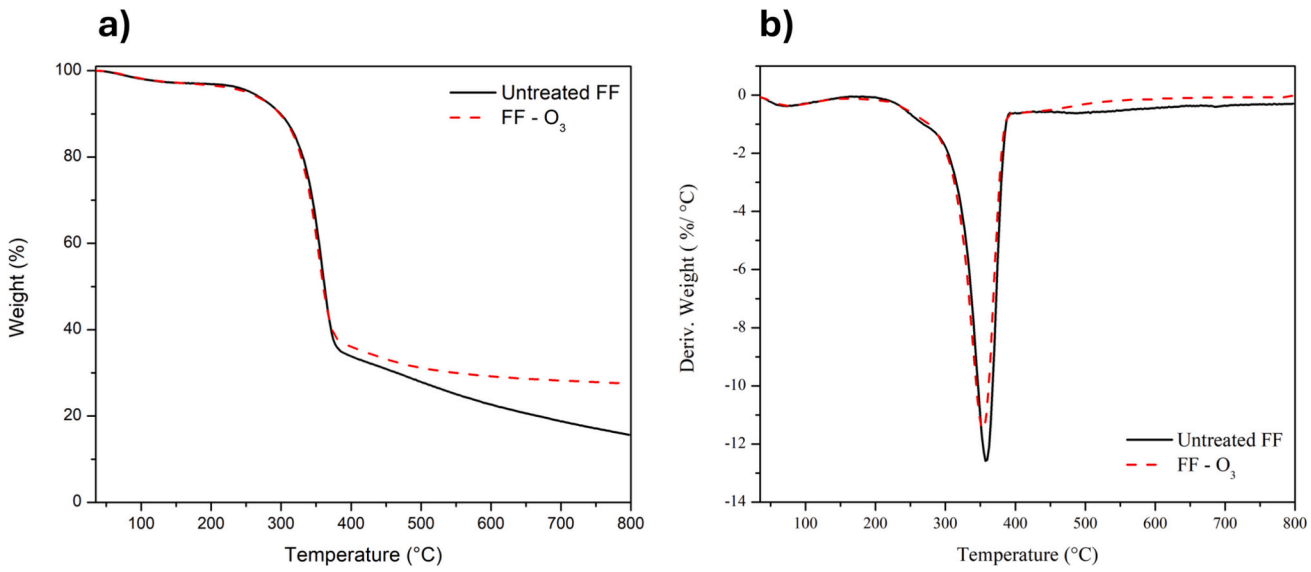


**Fig. 3.** (a) TGA and (b) DTG curves of untreated flax fiber (FF) and FF-$O_3$.

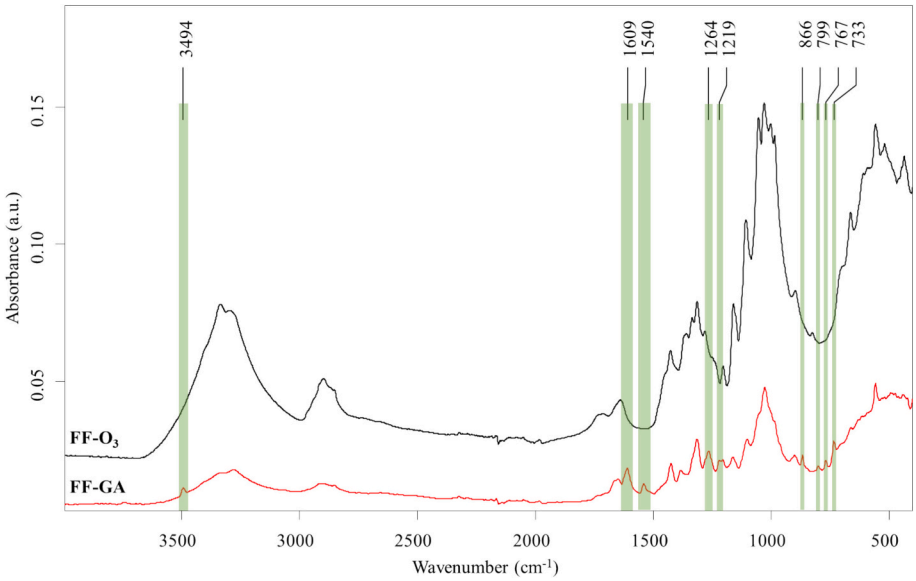


**Fig. 4.** Infrared spectra of FF-$O_3$ (black line) and FF-GA (red line).

(12.4 %) compared to FF-GA, due to the catalytic charring effect of iron phenylphosphonate. However, the small extent of this increase suggests a low loading of the flame-retardant complex on the fiber surface.

In addition, the onset degradation temperatures (Table S1) of both FF-GA and FF-GA-FeP were higher than those of FF. In particular, the increase in $T_{5\%}$ could be associated with the reduction in moisture content, while the presence of gallic acid and iron phenylphosphonate is responsible for the increase in $T_{10\%}$ values, due to their higher thermal stability (Figs. S2 and S3).

To further confirm the presence of paramagnetic iron in the FF-GA-FeP sample, the untreated and treated fibers were characterized by low-field NMR spectroscopy to evaluate the $^1$H longitudinal relaxation times ($T_1$) measured at the $^1$H Larmor frequency of 20.8 MHz. Indeed, the presence of paramagnetic species in proximity to $^1$H nuclei of the fibers can induce a shortening of $^1$H $T_1$ [62]. The $^1$H $T_1$ values of FF and FF-GA-FeP are reported in Fig. S4. It is worth noting that the $^1$H $T_1$ measured for FF-GA-FeP is slightly smaller than that of FF, confirming the incorporation of paramagnetic iron species into the fibers.

### 3.2. PLA-based composites characterization

#### 3.2.1. Thermal characterization of PLA-based composites

Fibers coated with the developed target complex (FF-GA-FeP) were used as reinforcement for PLA-based biocomposite materials (PLA/FF-FeP). Fig. 8 shows the TG and DTG curves of pure PLA, PLA reinforced with untreated flax fiber (PLA/FF), and PLA/FF-FeP, while Table 2 collects the thermogravimetric data.

Neat PLA undergoes a one-stage complete degradation between approximately 300 °C and 400 °C, with $T_{max}$ at 373.4 °C. The $T_{5\%}$, $T_{10\%}$, and $T_{max}$ of PLA/FF shift to lower temperatures compared to neat PLA, due to the cellulosic component of the raw FF that undergoes thermal degradation between 230 °C and 370 °C. FR-coated fiber-reinforced PLA exhibits slightly higher degradation temperatures compared to PLA/FF. To evaluate the charring efficiency of the hybrid FR, the residual weight of the composites was evaluated at 800 °C (Table 2). However, no significant change was observed in the residues of PLA/FF and PLA/FF-FeP, likely due to the limited coating amount on the fiber surface, as detected

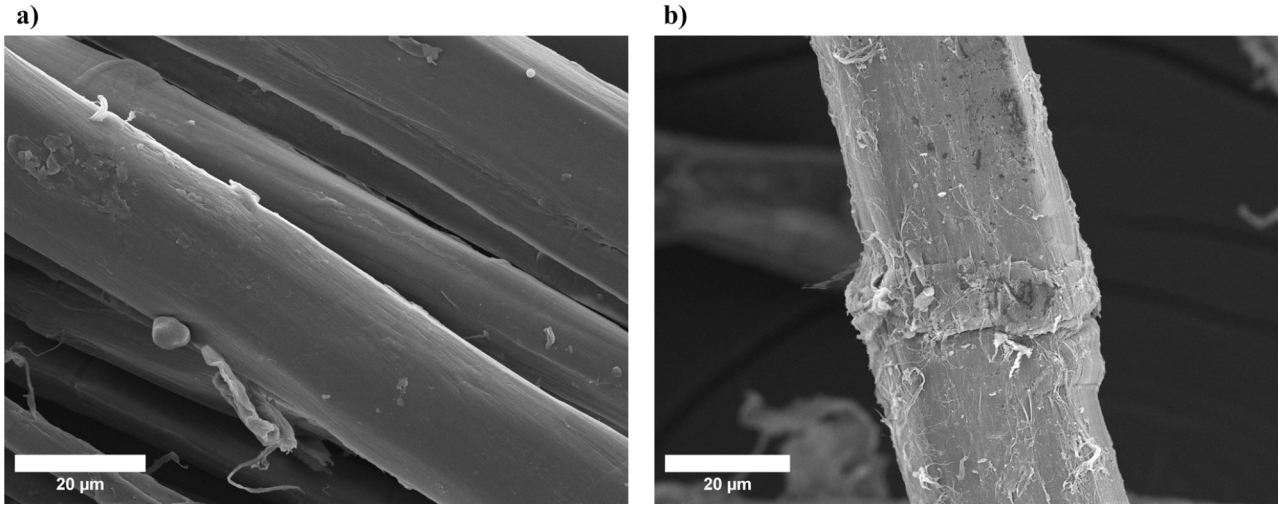


**Fig. 5.** SEM micrographs of (a) untreated flax fiber and (b) FF-GA.

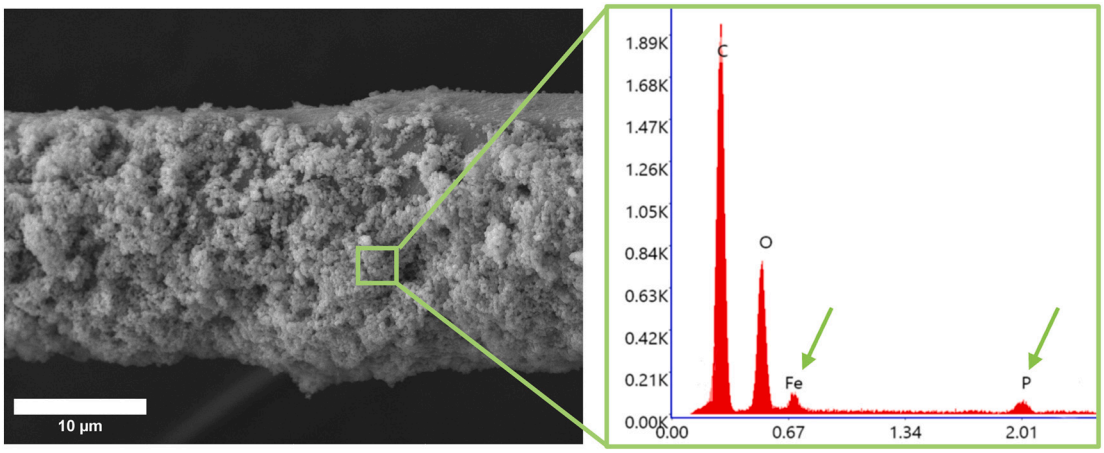


**Fig. 6.** SEM-EDS analysis of FF-GA-FeP.

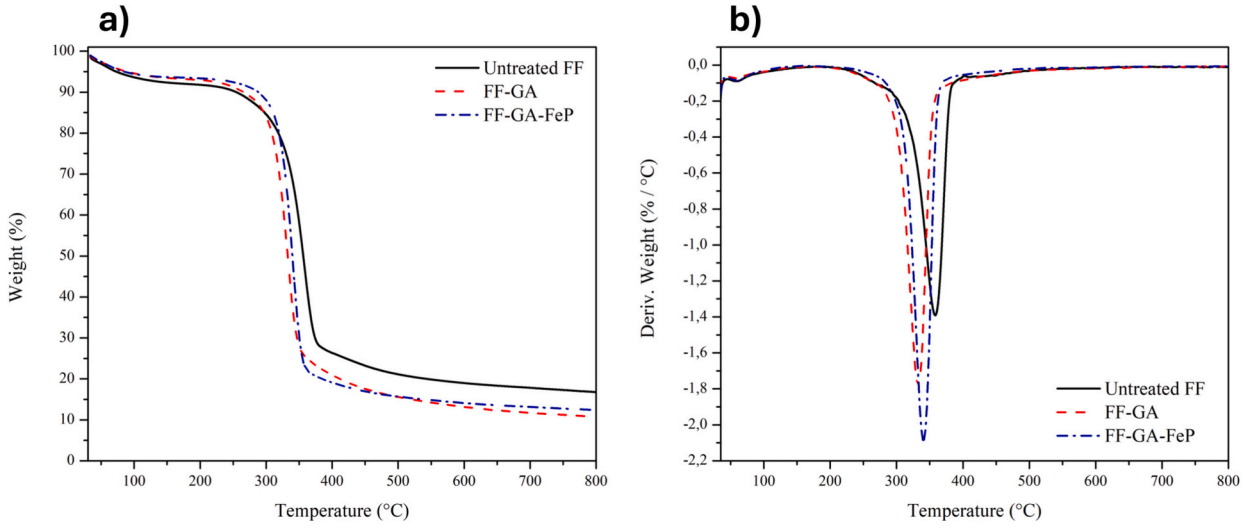


**Fig. 7.** (a) TG and (b) DTG curves of untreated FF, FF-GA and FF-GA-FeP.

by MP-AES analysis. Nonetheless, the developed FR complex, despite the low loading on the fiber surface, positively affected the thermal stability of FF-reinforced PLA composites.

DSC analyses were performed on pure PLA and its composites to investigate their thermal properties. The obtained parameters, including glass transition temperature ($T_g$), cold crystallization ($T_{cc}$) and melting

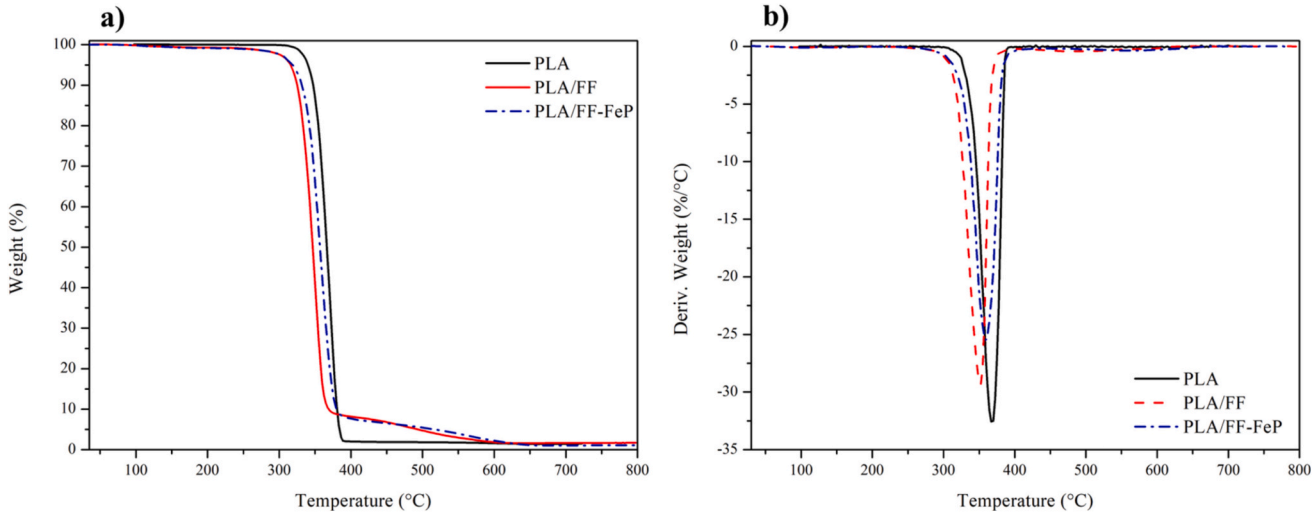


**Fig. 8.** (a) TG and (b) DTG curves of PLA, PLA/FF and PLA/FF-FeP.

**Table 2**
Onset temperatures evaluated at a weight loss of 5 % ($T_{5\%}$) and 10 % ($T_{10\%}$), maximum decomposition temperature ($T_{max}$) and weight residues at 800 °C (Residue) obtained from TGA measurements of PLA, PLA/FF, PLA/FF-FeP.

| Sample | $T_{5\%}$ (°C) | $T_{10\%}$ (°C) | $T_{max}$ (°C) | Residue (wt%) |
|---|---|---|---|---|
| PLA | 341.3 ± 1.1 | 348.8 ± 1.2 | 373.4 ± 2.1 | 1.1 ± 0.4 |
| PLA/FF | 308.4 ± 3.6 | 319.4 ± 3.3 | 350.9 ± 1.4 | 2.8 ± 0.3 |
| PLA/FF-FeP | 318.8 ± 0.3 | 331.3 ± 1.1 | 359.1 ± 0.1 | 2.6 ± 0.6 |

($T_m$) peak temperatures, are summarized in Table S2. In addition, the cold crystallization and melting enthalpy values were used for the determination of the degree of crystallinity ($\chi_c$) of the polymer.

The PLA/FF composite showed a $T_{cc}$ of 119.8 °C, slightly higher than neat PLA (115.2 °C). This enhancement can be attributed to the influence of FF on the molecular chain mobility of PLA. FF hinders the migration and diffusion of PLA molecular chains on the surface of the growing PLA crystals, thus affecting the formation of the crystal structure. Consequently, the cold crystallization temperature increases, and the overall crystallinity of PLA decreases [63,64]. In contrast, the PLA/FF-FeP composite showed a $T_{cc}$ of 118.8 °C, lower than PLA reinforced with untreated FF. This decrease suggests that the FR complex promotes the nucleation phase of the crystallization process. To further investigate this hypothesis, as-synthesized iron phenylphosphonate was added to neat PLA at a concentration of 1 wt% (PLA-FeP sample). DSC results showed a decrease in $T_{cc}$ for PLA-FeP (111.0 °C) compared with neat PLA, and a 65 % increase in $\chi_c$. This confirms that the developed complex acts as a nucleating agent. The hybrid FR, present in low loading on the fiber surface, had a negligible impact on the crystallinity of the PLA, hence favoring the decrease in $T_{cc}$ but not significantly affecting the overall crystallinity.

### 3.2.2. SSNMR characterization of PLA-based composites

The composites were also characterized by low-field SSNMR to evaluate if the paramagnetic iron present in the derivatized fibers (FF-GA-FeP) is still retained into the PLA/FF-FeP composite. To this purpose, $^1$H $T_1$ measurements were conducted on PLA/FF and PLA/FF-FeP composites and compared with those obtained with the FF and FF-GA-FeP fibers. The $^1$H $T_1$ values measured for PLA/FF and PLA/FF-FeP are reported in Fig. S5. For both samples, two values of $^1$H $T_1$ could be detected, a longer one ($T_{1,PLA}$) of about 550 ms, ascribable to the PLA matrix, and a shorter one ($T_{1,FF}$), of <100 ms, which was assigned to the reinforcing fibers. It is worth noting that $T_{1,FF}$ strongly resembles the $T_1$ values measured for FF and FF-GA-FeP, with $T_{1,FF}$ of PLA/FF-FeP being shorter than $T_{1,FF}$ of PLA/FF due to the presence of iron at the fibers' surface. These results suggest that the FR agent remains immobilized at the fibers' surface even after composite preparation.

### 3.2.3. Fire behavior of PLA-based composites

The flame-retardant properties of the developed FR coating complex were analyzed by flammability (LOI and UL-94) and cone calorimetry tests (CCT); the latter is a widely accepted method for evaluating the combustion behavior of materials under conditions close to a real fire scenario [65]. Table S3 collects the results from the flammability tests. First, it is worth noting that the modification of the flax fibers accounted for a limited increase in the LOI value, which moved from 20.3 to 20.8 %. Furthermore, all the specimens, irrespective of the modification of the flax fibers, could not be classified in vertical flame spread tests. Indeed, the applied flame reached the holding clamp very quickly, meanwhile providing a significant dripping of incandescent drops that ignited cotton batting. Table S4 summarizes the key parameters of CCT tests evaluated for PLA/FF and PLA/FF-FeP composites. The results revealed several notable findings. First, the time to ignition (TTI) of PLA/FF-FeP composites exhibited a slight increase compared to untreated FF-reinforced PLA. Additionally, the peak of heat release rate (pHRR) underwent a 7 % decrease. Most significantly, both total smoke release (TSR) and specific extinction area (SEA) of the FR-coated fiber-reinforced composites remarkably lowered (by 87 and 68 %, respectively) compared to PLA/FF counterparts. These findings indicate the substantial suppression of smoke generation and flame spread, which are critical factors in fire safety. In particular, also considering that final residue of the cone calorimetry tests for the composites containing the treated fibers is lower than that of untreated counterpart, it can be assumed that the surface treatment of the fibers is active mainly in the gas phase, through the formation of phosphorus containing radicals that are capable of entrapping the radical species propagating the flame. Besides, the possible formation of ferric oxide during the decomposition of the flame retarded fibers during the exposure to the irradiative heat flux may account for the smoke reduction, because it is well known to be an effective smoke suppressant [66–68]. A representative illustration is shown in Fig. 9.

Moreover, the fire propagation index (FPI), calculated as the ratio of pHRR to TTI, turns out to be lower for PLA/FF-FeP than for PLA/FF. This result points out that the modified FF composite tends to be less prone to fire propagation. Interestingly, all these enhancements are achieved in the presence of low FR coating loadings on the fiber surface, hence demonstrating its flame-retardant effectiveness.

Importantly, in accordance with thermogravimetric and MP-AES

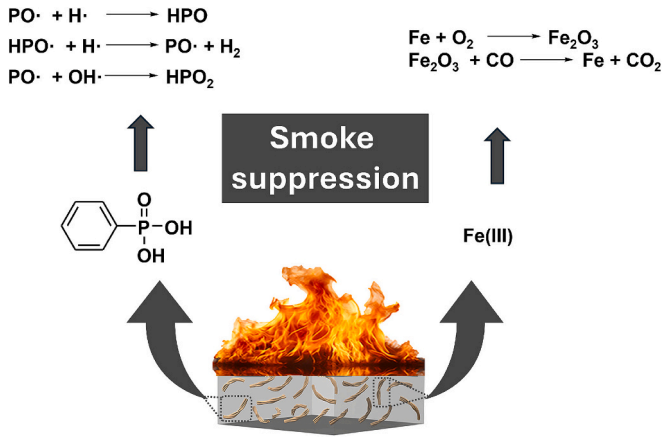


**Fig. 9.** Schematic illustration of the proposed mechanism of FR coated flax fiber.

analyses, the low FR loading on the fiber's surface does not lead to a substantial reduction in mass loss attributable to char formation (Table S4).

Gaseous products generated during thermal degradation of composites were identified by TG-FTIR analysis. Fig. 10a–c present the 3D plots of the evolved gas products for PLA, PLA/FF, and PLA/FF-FeP, respectively. Fig. 11 shows the infrared spectra of PLA and its composites at the temperature corresponding to the maximum decomposition rate ($T_{max}$) versus the total absorbance intensity of the gaseous products. The signal between 4000 $cm^{-1}$ and 3500 $cm^{-1}$ was attributed to water generated during pyrolysis. Furthermore, absorbances due to the presence of acetaldehyde generated by intramolecular transesterification reactions during thermal degradation of PLA were observed. In particular, signals were observed at 2738 $cm^{-1}$ (aldehydic C—H stretching) [69], at 1762 $cm^{-1}$ (carbonyl group C═O stretching) [70] and between 3000 and 2750 $cm^{-1}$ (C—H aliphatic stretching) [71]. Besides, signals at 1456 and 1373 $cm^{-1}$ were associated with the C—H bending of $CH_3$ [72]. C—O stretching (1300 $cm^{-1}$ to 1000 $cm^{-1}$), carbonyl group C═O stretching (1762 $cm^{-1}$), C—H bending and stretching of methyl groups (1456 $cm^{-1}$, 1373 $cm^{-1}$) and the ring skeletal vibration (933 $cm^{-1}$) indicate the presence of lactide or cyclic oligomeric species among the products evolved from the thermal degradation of PLA [72,73], which can be generated by either radical or esterification processes [74].

The presence of carbon dioxide ($CO_2$), a major homolytic thermal degradation product of the PLA chain, is indicated by the appearance of two bands at 2359 $cm^{-1}$ and 2322 $cm^{-1}$ [75], while carbon monoxide (CO), generated by the transesterification reaction, is identified by signals at 2178 and 2115 $cm^{-1}$, which correspond to the bending of the C—O bonds [76].

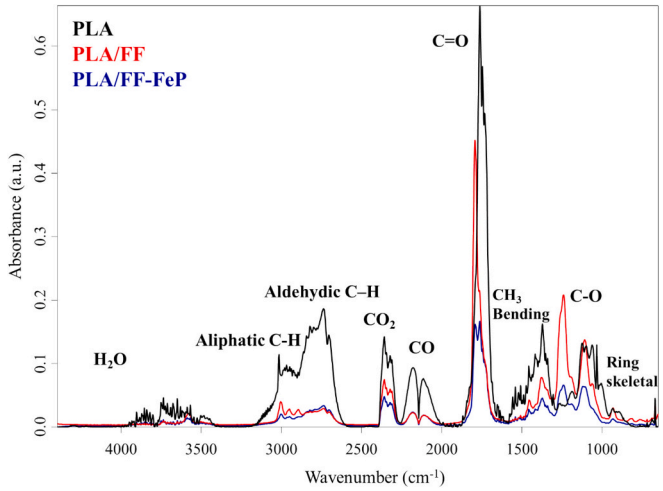


**Fig. 11.** Infrared spectra of gas products from PLA (black line), PLA/FF (red line) and PLA/FF-FeP (blue line) at $T_{max}$.

In the PLA/FF spectrum, a decrease in signals associated with CO and acetaldehyde production was observed. The scientific literature reports that the reinforcement of PLA with lignocellulosic fiber can promote the occurrence of radical reactions in PLA during pyrolysis by favoring the degradation of lignin component while limiting the transesterification reactions responsible for the production of CO and acetaldehyde [77,78]. Further, there is an increase in the signal at 1241 $cm^{-1}$, attributable to various organic compounds containing C—O bonds, such as carboxylic acids, alcohols, anhydrides, and esters [79], which are by-products generated in the presence of FF.

On the other hand, the spectrum of PLA/FF-FeP shows a decrease in absorbances associated with lactide or cyclic oligomer (including C—H bending and stretching of methyl groups, C═O stretching of carbonyl group, C—O stretching, and ring skeletal vibration) and $CO_2$ compared to PLA/FF. This suggests that the FR coating may affect the radical process during the co-pyrolysis of PLA/FF.

Therefore, TG-FTIR results confirm that even if the FR coating is present in low loading on the fiber surface, it exhibits flame retardant effectiveness.

### 3.2.4. *Preliminary characterization of the mechanical behavior of PLA-based composites*

To evaluate the effect of ozone treatment and FR coating on the mechanical properties of the composite, some preliminary tensile tests were conducted; the results as stress-strain curves for PLA, PLA/FF, PLA/FF-$O_3$, and PLA/FF-FeP are shown in Fig. 12. In the presence of FF, there is a noticeable embrittlement of the material, as evidenced by the

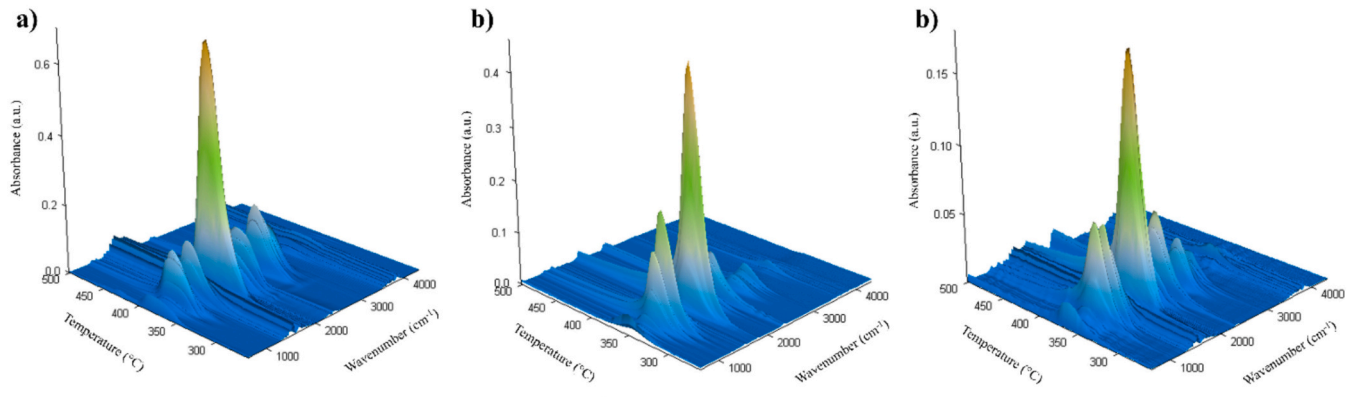


**Fig. 10.** 3D TG-FTIR plots of (a) PLA, (b) PLA/FF and (c) 3D PLA/FF-FeP.

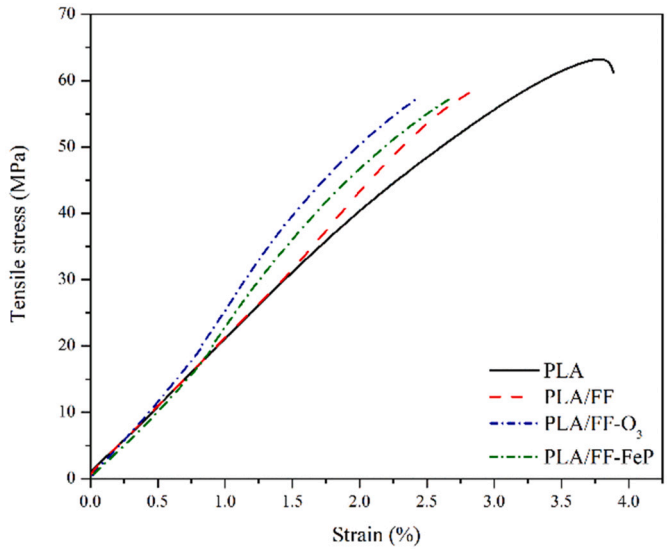


**Fig. 12.** Tensile test results of PLA, PLA/FF, PLA/FF-O3 and PLA/FF/FeP.

lowering of strain at break, together with a decrease in tensile strength. The tensile strength of the neat PLA was equal to 63.9 (± 2.1) MPa, while the tensile strengths for PLA/FF, PLA/FF-$O_3$, and PLA/FF-FeP were found to be 59.9 (± 2.4) MPa, 56.7 (± 0.8) MPa, and 56.9 (± 1.5) MPa, respectively. These findings are consistent with several studies in the literature, which highlighted a worsening in the mechanical properties of polymers after the incorporation of plant fibers, because of poor reinforcement-matrix interfacial adhesion and fiber agglomeration as fiber content increases [80,81].

It is important to note that the $O_3$ pretreatment of FF, along with the subsequent coating with FeP, contributed to a further reduction (5.3 %) compared to PLA/FF. In this case, this result could be ascribed to the effect of $O_3$ on lignin structure, as previously assessed by thermogravimetric analysis. Moreover, the addition of 20 wt% flax fibers in PLA/FF promoted an increase in Young's modulus from 1.9 (± 0.2) to 2.7 (± 0.2) GPa for PLA and PLA/FF, respectively. PLA reinforced with ozone-pretreated fibers (2.8 (± 0.3) GPa) maintained stiffness akin to PLA/FF, whereas PLA/FF-FeP exhibited a Young's modulus of 3.1 (± 0.2) GPa, with a slight stiffness increment compared to PLA/FF-$O_3$. This finding suggests an enhanced fiber stiffness due to the presence of the hybrid FR coating, resulting in an increase in the Young's modulus of the composite.

Fig. 13 depicts SEM micrographs of the fracture surfaces of PLA/FF and PLA/FF-FeP composites after tensile tests. Examination revealed poor interfacial adhesion between untreated flax fibers and the PLA matrix, evidenced by clean fiber surfaces and prevalent failure modes such as pull-out and debonding (Fig. 13a). Similar characteristics were observed in the fracture surface of PLA/FF-FeP, albeit with indications of mild interfacial adhesion between fibers and the matrix, as shown by covered fiber surfaces and connection points with the polymer matrix (Fig. 13b). It is, thus, hypothesized that the FR coating might improve the adhesion between flax fibers and PLA, although the low loading and non-uniformity of GA-FeP complex on the fiber surfaces could mask this effect during quasi-static mechanical tests.

Aiming to confirm that the results of the mechanical tests on the composites are specifically influenced by the properties of the treated fibers, tensile tests were performed on flax fabrics that underwent similar modification steps as the short fibers used as reinforcements in PLA. The breaking forces measured were 342 (± 34) N, 301 (± 38) N, and 226 (± 26) N for untreated flax fabric, flax fabric-$O_3$, and flax fabric-GA-FeP, respectively.

The $O_3$ treatment led to a decrease in tensile strength (around −12 % with respect to neat fabric) because of the aforementioned action on the lignin component, whose removal contributes to reducing the tensile performance of the flax fibers [82].

On the other hand, $O_3$ treatment could also affect the crystal structure of the flax fabric cellulosic component. Cellulose is a high-molecular weight linear chain polymer containing three hydroxyl groups for each glucose residue unit [83]. These hydroxyl groups form extensive intra- and inter-molecular hydrogen bond networks, and the formation of van der Waals forces between adjacent cellulose molecules is also allowed [84]. The combination of these interactions gives rise to ordered crystalline arrangements. Several studies in the literature have explored the relationship between tensile properties and the cellulose crystallinity index (CI) in natural fibers, identifying an increase in tensile strength and Young's modulus as the crystallinity index increases [85]. $O_3$ treatment converts the primary hydroxyl groups of celluloses into carboxyl groups, potentially altering the interactions and thus the crystal structure of cellulose [86].

Flax fabric-GA-FeP showed a decrease in breaking force compared with untreated and $O_3$-treated flax fabrics, by 33 and 25 %, respectively. Fabric coating occurs in two main steps: (i) the first involved immobilization of gallic acid units by immersion of the fabric in the galloyl chloride/TAME mixture; (ii) the second required the complexation of

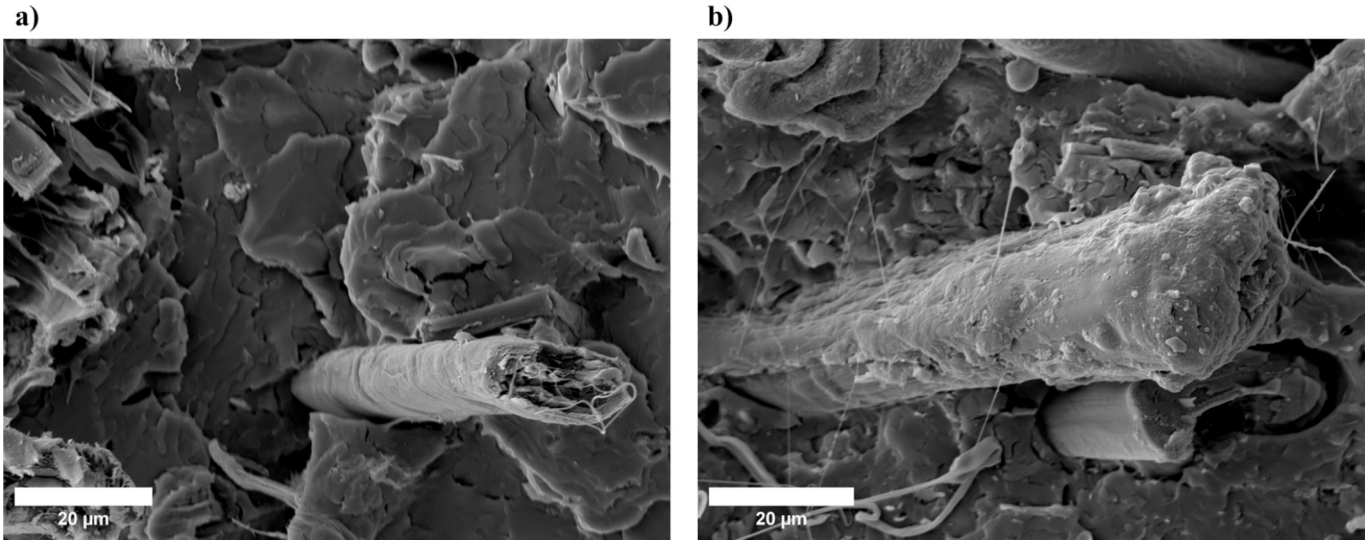


**Fig. 13.** SEM micrographs of fractured surfaces of (a) PLA/FF and (b) PLA/FF-FeP.

iron phenylphosphonate by reaction with $FeCl_3$ and PPA in water. Both steps, however, expose the fiber to HCl, which is produced as a by-product in the first step and originates from the dissociation of $FeCl_3$ in $H_2O$ during the second step. The exposure of fibers to an acidic environment could catalyze the cleavage of β-1,4-glycosidic bonds between two D-anhydroglucosepyranose units, resulting in a reduction of the cellulosic chain's degree of polymerization, thereby potentially lowering the mechanical properties [87,88]. Furthermore, the FR complex was immobilized on the fiber via anhydride bonds by exploiting the carboxyl groups of the cellulosic component, resulting in a possible change of the crystal structure [89,90]. Therefore, the reduction in mechanical properties is likely to be due to an alteration in the crystal structure of the cellulosic component of the flax fiber.

To assess whether the reduction in the mechanical properties observed in flax fabric-$O_3$ and flax fabric-GA-FeP are ascribable to the change in the cellulose crystal structure, untreated flax fabric, flax fabric-$O_3$, flax fabric-GA, and flax fabric-GA-FeP were analyzed by scanning SAXS/WAXS/Absorption microscopy. In Fig. 14, representative micro-diffraction data collected at the XMI-Lab in the wide (μWAXS 2D patterns) and small (composite μSAXS microscopies) angle scattering ranges, are reported for untreated and $O_3$-treated flax fabrics, the results being similar for GA-FeP- and GA-treated flax samples (see also Fig. S6).

SAXS scanning microscopies clearly show the texture of the fabrics, being the preferred azimuthal orientation of the μSAXS intensity represented by suitable colors, according to the reference color wheels, directly related (i.e. perpendicular) to the orientation of the flax fibers. On the other hand, no features relevant to possible nanoscale order in the accessible range of length scales (about 3 ÷ 100 nm) were detected in the μSAXS patterns (not shown). Micro-WAXS (μWAXS) patterns, representative of the atomic structure, were collected at selected sample positions, to investigate possible local structural variations within each sample and between different samples, and to relate the molecular structure to fiber orientation. The μWAXS patterns reported in Fig. 14 were collected at selected points of the single yarns, clearly showing that flax yarns feature a well-defined crystallographic orientation with respect to the fiber axis; the 2D WAXS pattern thus rotates according to the single yarn orientation across the fabric. Both crystallographic orientations overlap in the positions of fabric "nodes" (Fig. S7), where crossing yarns overlap. Therefore, based on the comparison between experimental and calculated patterns for different cellulose polymorphs (Fig. S8), flax atomic structure has been determined to be compatible for all samples with cellulose $I_\alpha/I_\beta$, as the main crystalline components (hard to distinguish because of peak overlap [91]), with triclinic unit cell, and minor contributions from cellulose II and III [92,93], with monoclinic unit cell. Cell parameters were derived for $I_\alpha/I_\beta$ ($a = 7.204$ Å; $b = 6.596$ Å; $c = 11.41210$ Å; $\alpha = 119.285°$; $\beta = 114.988°$; $\gamma = 78.377°$) and cellulose II/III ($a = 4.450$ Å; $b = 7.850$ Å; $c = 10.330$ Å; $\alpha = 90.00°$; $\beta = 90.00°$; $\gamma = 105.10°$), by fitting a representative 1D-folded WAXS pattern of the untreated flax sample by using the program EXPO [94] (Fig. S9). Based on Figs. 14, S6, and S7, the $I_\alpha/I_\beta$ component shows a preferred orientation of the main WAXS signals perpendicular to the fiber axis; on the other hand, the cellulose II/III component features a much wider azimuthal distribution of the crystalline domains' orientations. The II/III component could act as a compacting filler for the main $I_\alpha/I_\beta$ fiber template. Further, the average WAXS patterns were collected for each sample simultaneously with the relevant SAXS microscopy and showed no significant variations after $O_3$ pretreatment or FR coating treatments. As a final confirmation of the local structural invariance across all fabrics, full WAXS scanning microscopies were collected afterward by using the XENOCS equipment with a highly performing 1 M

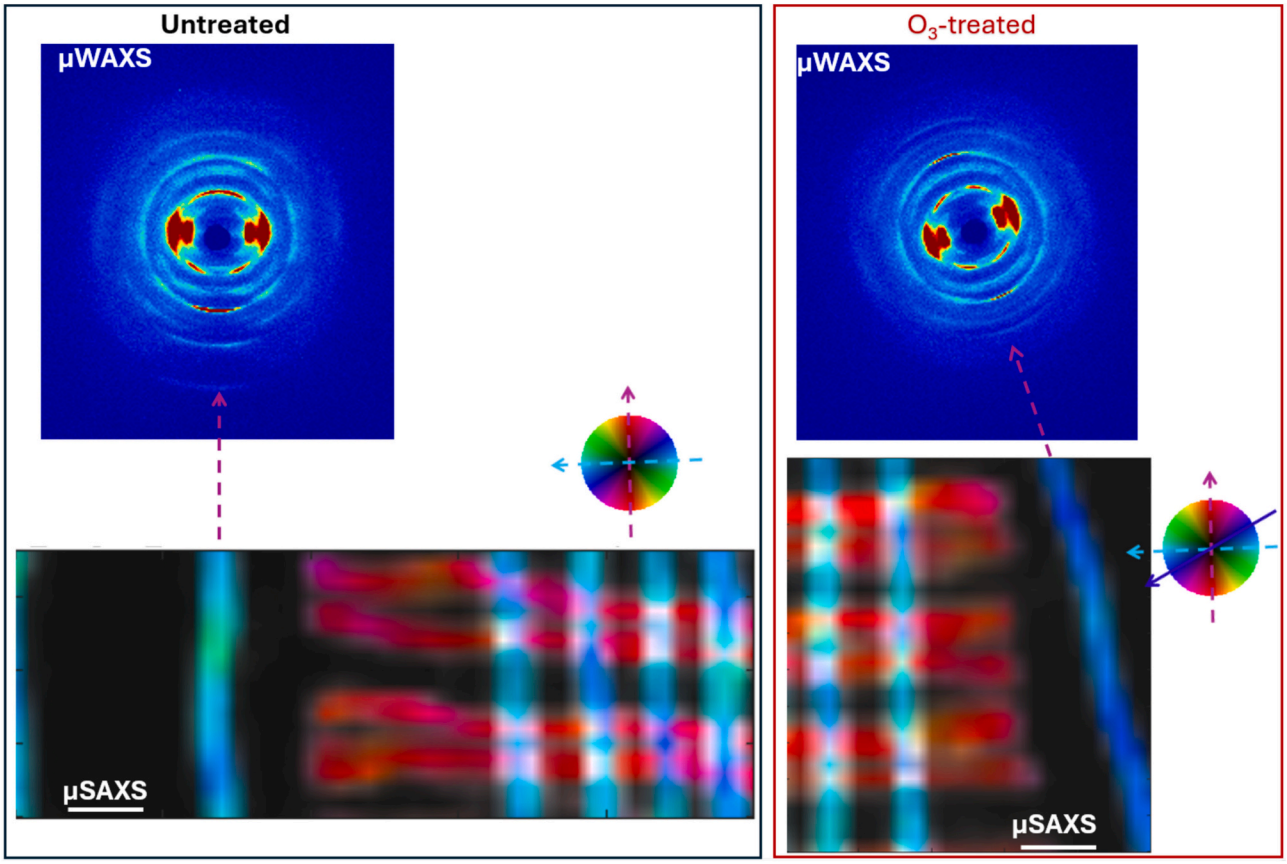


**Fig. 14.** Representative micro-diffraction data in the wide (μWAXS 2D patterns) and small (composite μSAXS microscopies) angle scattering ranges, respectively, for untreated and $O_3$-treated flax fabrics. The white scale bars in the μSAXS microscopies are 1 mm long. The color in each angular sector of the wheels indicates a preferred orientation of the SAXS signal; the superimposed arrows indicate the main orientations detected in each sample.

Eiger detector (DECTRIS). The results revealed no changes in the crystalline structure of the cellulosic component of flax fabric resulting from either $O_3$ pre-treatment or FR coating treatment all over the investigated sample areas. Only slight shifts were locally detected, due to sample mounting and conformation, which affect data calibration and hence the derived unit cell parameters (Fig. S10).

In addition, for further insight, also FR-coated short fibers were characterized to assess potential changes in their crystallinity. Untreated FF, FF-GA and FF-GA-FeP were analyzed using SSNMR spectroscopy. SSNMR is a well-established technique for the characterization of cellulose-based materials to assess the presence of amorphous and crystalline phases and to evaluate their degree of crystallinity [95–97]. For all samples, high-resolution $^{1}H$-$^{13}C$ cross-polarization (CP) spectra recorded under magic angle spinning (MAS) exhibit the characteristic signals of cellulose (Fig. S11), also allowing for the differentiation of $^{13}C$ signals originating from both the crystalline and amorphous phases of the sample. Despite the non-quantitative nature of CP experiments, the relative intensity of all signals remains unaltered upon derivatization, suggesting that the chemical treatment does not perturb the crystallinity of the flax fibers.

To quantify the crystalline and amorphous phase of the samples, on-resonance $^{1}H$ free induction decays (FIDs) were acquired using a low-field NMR spectrometer. Indeed, $^{1}H$ FIDs profile depends on the transverse relaxation times $T_2$ of $^{1}H$ nuclei. Depending on the molecular mobility of the $^{1}H$ nuclei, $T_2$ monotonically increases with the degree of mobility of each fraction of the sample, allowing us to distinguish between the amorphous and crystalline phases present in the sample [97]. The analysis of $^{1}H$ FIDs was conducted using a linear combination of decay functions characterized by different $T_2$ values and different weights, each ascribable to regions of the sample with different molecular mobility. For all fiber samples, the decay ascribable to the crystalline and the amorphous component was reproduced by an Abragamian and a Gaussian function, respectively; an exponential function was also added to reproduce a more mobile component with longer $T_2$, ascribable to adsorbed water. Fig. S12a shows the $^{1}H$ FIDs obtained for FF, FF-GA, and FF-GA-FeP, where no significant differences can be detected among the samples. From the analysis of the decay, most protons (82–85 %) belong to the crystalline phase, with 6–7 % belonging to the amorphous phase and 9–11 % ascribable to adsorbed water (Fig. S12b–c). These results confirm that the fibers' crystallinity is practically unaffected by the surface modification, as also suggested by $^{1}H$-$^{13}C$ CP SSNMR and as observed for FR-coated fabrics analyzed by WAXS.

Therefore, the observed reduction in maximum force of $O_3$ pre-treated fabric and the consequent decrease in tensile strength of the PLA/FF-$O_3$ composite compared to untreated flax fabric and PLA/FF, respectively, is likely to be associated with the ozone-induced degradation of lignin structure, as the crystallinity of cellulose is not affected by the pretreatment. The decrease in breaking force observed in flax fabric-GA-FeP is also not attributable to changes in the crystal structure of cellulose. It is important to consider that flax fiber includes not only cellulose but also significant proportions of hemicelluloses (12–15 %) and pectin (1.4–5.7 %) [98]. Previous studies reported that both components, given their structure, can be hydrolyzed under acidic conditions [99,100]. Flax fiber can be considered as a composite itself, in which cellulose microfibrils, coated with hemicelluloses, are embedded in a pectin matrix [101]. Research in the literature highlighted a correlation between the cell wall composition—specifically the hemicellulose/pectin ratio—and the stress-strain behavior of the fiber, as these polysaccharides influence the reorientation of cellulose microfibrils during tensile testing [102].

In particular, variation in the amounts of hemicellulose and pectin can lead to changes in the microfibrillar angle (MFA) in the flax fiber structure. Therefore, these polysaccharides mainly affect the Young's modulus of the fiber, while a clear and direct correlation between MFA and strength at break has not been identified, which at variance appears to be more closely related to the cellulosic component [103].

Morphological changes, such as structural integrity, surface roughness, or fiber diameter can lead to a decrease in the breaking force [104].

Therefore, the fiber coated with the hybrid FR was examined by SEM, as depicted in Fig. 15. Although the coating does not allow a direct inspection of the fiber morphology, it was possible to identify regions of uncoated fibers that showed direct damage of the fiber surface. In addition, regions of fiber showing FR coating damage were also identified. These defects may influence the stress distribution along the fiber, acting as localized stress concentration points and thereby promoting fiber failure (Fig. 15a). Natural fibers such as flax are characterized by a highly heterogeneous structure presenting inherent defects, such as kink bands and microcompressions, which affect the fiber's mechanical properties [105]. Moreover, studies reported that kink bands, besides being preferential sites for crack initiation [106], are also more chemically reactive regions of the fiber [107]. This phenomenon was also evident in SEM micrographs, where kink regions abundantly coated by the FR complex can be observed. It is therefore assumed that these regions are highly susceptible to crack propagation due to both the inherent fiber defects and the possibility of coating damage in these areas (Fig. 15b). This could explain the reduction in the maximum tensile force observed in flax fabric-GA-FeP compared to its untreated counterpart.

Interestingly, despite the FR-coated fabric exhibited reduced tensile properties compared to the flax fabric-$O_3$, the tensile strength was not significantly worsened in the composite. Conversely, a slight increase in Young's modulus of PLA/FF-FeP compared to PLA/FF-$O_3$ was observed. These results could support the hypothesis that FR coating may affect fiber-matrix interaction, an effect counteracted by the decrease in fiber strength.

## 4. Conclusions

A sustainable method for functionalizing flax fibers with an organic-inorganic hybrid flame retardant was successfully developed. The bio-inspired coating process enabled the immobilization of iron phenylphosphonate on the fiber surface, using mild reaction temperatures and exploiting green solvents such as TAME and $H_2O$.

The coated fibers were employed for preparing PLA-based composites: despite the low loading of the FR coating on the fiber surface, thermogravimetric analyses revealed an increase in thermal stability, while cone calorimetry tests showed a decrease in pHRR by 7 %, and a substantial decrease in total smoke production by 87 % and in specific extinction area by 68 % compared to the untreated flax reinforced composite. TG-FTIR analysis suggested that FR coating could influence the radical process of co-pyrolysis in the PLA/FF-FeP composite.

Compared to neat flax fabric, $O_3$-pretreated fabric tensile test showed a breaking force reduction of 12 %, significantly lower than 33 % reduction of FR-coated fabric. However, PLA reinforced with $O_3$-pretreated fabric and FR-coated fabric exhibited comparable tensile strength. These findings suggest a FR-coating effect on fiber-matrix interaction, as confirmed by SEM micrographs of fractured surfaces. Nevertheless, this effect was counterbalanced by a reduction in fiber tensile strength due to the coating process.

Future work will modify the coating process by reducing treatment duration to minimize fiber damage and optimizing GA unit fiber functionalization. These changes aim to ensure a more uniform coating and reduce stress concentrations from coating defects.

## CRediT authorship contribution statement

**Alessia Pantaleoni:** Writing – original draft, Visualization, Validation, Investigation, Conceptualization. **Assunta Marrocchi:** Writing – review & editing, Supervision, Methodology, Conceptualization. **Pietro Russo:** Writing – review & editing, Investigation. **Giulio Malucelli:** Writing – review & editing, Investigation. **Davide Altamura:** Writing – original draft, Investigation. **Francesca Nardelli:** Writing – original

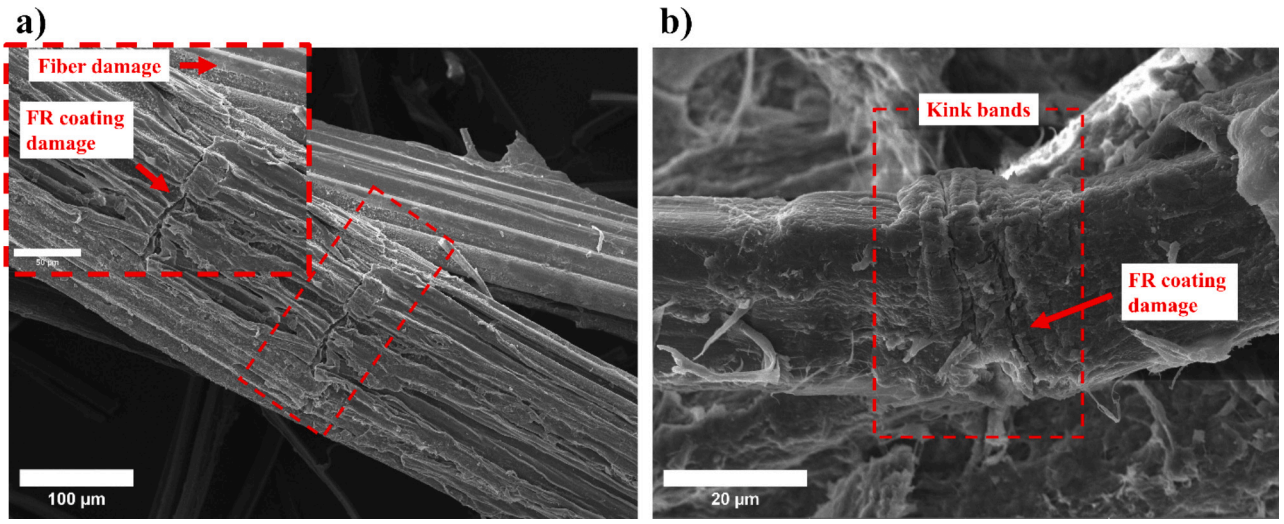


**Fig. 15.** SEM micrographs of flax fabric-GA-FeP showing (a) fabric and coating damage and (b) morphology of coated fabric in kinks bands.

draft, Investigation. **Silvia Pizzanelli:** Writing – review & editing. **Angelo Freni:** Writing – review & editing. **Cinzia Giannini:** Writing – review & editing, Funding acquisition. **Maria Laura Santarelli:** Writing – review & editing, Resources. **Irene Bavasso:** Writing – review & editing, Validation, Methodology, Investigation. **Maria Paola Bracciale:** Writing – review & editing, Supervision, Methodology, Conceptualization. **Fabrizio Sarasini:** Writing – review & editing, Supervision, Resources, Funding acquisition, Conceptualization.

## Declaration of competing interest

The authors declare the following financial interests/personal relationships which may be considered as potential competing interests: Fabrizio Sarasini reports financial support was provided by European Union - NextGenerationEU. Cinzia Giannini reports financial support was provided by European Union - NextGenerationEU. If there are other authors, they declare that they have no known competing financial interests or personal relationships that could have appeared to influence the work reported in this paper.

## Acknowledgments

Financed by the European Union - NextGenerationEU (National Sustainable Mobility Center CN00000023, Italian Ministry of University and Research Decree n. 1033 - 17/06/2022, Spoke 11 - Innovative Materials & Lightweighting). The opinions expressed are those of the author only and should not be considered as representative of the European Union or the European Commission's official position. Neither the European Union nor the European Commission can be held responsible for them. D. A. and C. G. acknowledge Dr. Carlotta Giacobbe (XENOCS) and Dr. Francesco Scattarella for their support in WAXS data collection and microscopy reconstruction, respectively, and support from the PNRR infrastructure project "Potentiating the Italian Capacity for Structural Biology Services in Instruct Eric (ITACA.SB)" (Project No. IR0000009, CUP B53C22001790006) within the call MUR 3264/2021 PNRR M4/C2/L3.1.1, funded by the European Union NextGenerationEU.

## Appendix A. Supplementary data

Supplementary data to this article can be found online at https://doi.org/10.1016/j.ijbiomac.2025.140215.

## Data availability

Data will be made available on request.

## References

[1] S. Prashanth, S. Km, K. Nithin, S. Sachhidananda, Fiber reinforced composites -a review, J. Mater. Sci. Eng. 6 (2017) 341, https://doi.org/10.4172/2169-0022.1000341.
[2] C. Böhringer, The Kyoto Protocol: a review and perspectives, Oxf. Rev. Econ. Policy 19 (2003) 451–466, https://doi.org/10.1093/OXREP/19.3.451.
[3] G. Rajeshkumar, S. Arvindh Seshadri, G.L. Devnani, M.R. Sanjay, S. Siengchin, J. Prakash Maran, N.A. Al-Dhabi, P. Karuppiah, V.A. Mariadhas, N. Sivarajasekar, A. Ronaldo Anuf, Environment friendly, renewable and sustainable poly lactic acid (PLA) based natural fiber reinforced composites – a comprehensive review, J. Clean. Prod. 310 (2021) 127483, https://doi.org/10.1016/j.jclepro.2021.127483.
[4] P. McKeown, M.D. Jones, The chemical recycling of PLA: a review, Sustain. Chem. 1 (2020) 1–22, https://doi.org/10.3390/suschem1010001.
[5] R. Siakeng, M. Jawaid, H. Ariffin, S.M. Sapuan, M. Asim, N. Saba, Natural fiber reinforced polylactic acid composites: a review, Polym. Compos. 40 (2019) 446–463, https://doi.org/10.1002/pc.24747.
[6] V. Mazzanti, R. Pariante, A. Bonanno, O. Ruiz de Ballesteros, F. Mollica, G. Filippone, Reinforcing mechanisms of natural fibers in green composites: role of fibers morphology in a PLA/hemp model system, Compos. Sci. Technol. 180 (2019) 51–59, https://doi.org/10.1016/j.compscitech.2019.05.015.
[7] F. Sbardella, I. Rivilla, I. Bavasso, P. Russo, L. Vitiello, J. Tirillò, F. Sarasini, Zinc oxide nanostructures and stearic acid as surface modifiers for flax fabrics in polylactic acid biocomposites, Int. J. Biol. Macromol. 177 (2021) 495–504, https://doi.org/10.1016/j.ijbiomac.2021.02.171.
[8] T. Yu, C. Hu, X. Chen, Y. Li, Effect of diisocyanates as compatibilizer on the properties of ramie/poly(lactic acid) (PLA) composites, Compos. Part A Appl. Sci. Manuf. 76 (2015) 20–27, https://doi.org/10.1016/j.compositesa.2015.05.010.
[9] A. Khan, S.M. Sapuan, J. Yusuf, V.U. Siddiqui, E.S. Zainudin, M.Y.M. Zuhri, B.T. H. Tuah Baharuddin, M.A. Ansari, A.A.A. Rahman, An examination of cutting-edge developments in bamboo-PLA composite research: a comprehensive review, Renew. Sust. Energ. Rev. 188 (2023) 113832, https://doi.org/10.1016/j.rser.2023.113832.
[10] J. Holbery, D. Houston, Natural-fiber-reinforced polymer composites in automotive applications, Jom 58 (2006) 80–86, https://doi.org/10.1007/s11837-006-0234-2.
[11] S.K. Mary, M.S. Thomas, R.R. Koshy, P.K.S. Pillai, L.A. Pothan, S. Thomas, Adhesion in biocomposites: a critical review, Prog. Adhes. Adhes. 6 (6) (2021) 531–558, https://doi.org/10.1002/9781119846703.ch11.
[12] M. Yasir Khalid, R. Imran, Z. Ullah Arif, N. Akram, H. Arshad, A. Al Rashid, F. Pedro García Márquez, Developments in Chemical Treatments, Manufacturing Techniques and Potential Applications of Natural-fibers-based Biodegradable Composites, 2021, https://doi.org/10.3390/coatings11030293.
[13] S. Borysiak, A. Grząbka-Zasadzińska, M. Odalanowska, A. Skrzypczak, I. Ratajczak, The effect of chemical modification of wood in ionic liquids on the supermolecular structure and mechanical properties of wood/polypropylene composites, Cellulose 25 (2018) 4639–4652, https://doi.org/10.1007/s10570-018-1892-2.
[14] T. Lu, M. Jiang, Z. Jiang, D. Hui, Z. Wang, Z. Zhou, Effect of surface modification of bamboo cellulose fibers on mechanical properties of cellulose/epoxy

composites, Compos. B Eng. 51 (2013) 28–34, https://doi.org/10.1016/j.compositesb.2013.02.031.
[15] W.S. Chow, E.L. Teoh, J. Karger-Kocsis, Flame retarded poly(lactic acid): a review, Express Polym Lett 12 (2018) 396–417, https://doi.org/10.3144/expresspolymlett.2018.34.
[16] M.W. Chai, S. Bickerton, D. Bhattacharyya, R. Das, Influence of natural fibre reinforcements on the flammability of bio-derived composite materials, Compos. B Eng. 43 (2012) 2867–2874, https://doi.org/10.1016/j.compositesb.2012.04.051.
[17] R. Gupta, M.K. Singh, S.M. Rangappa, S. Siengchin, H.N. Dhakal, S. Zafar, Recent progress in additive inorganic flame retardants polymer composites: degradation mechanisms, modeling and applications, Heliyon 10 (2024), https://doi.org/10.1016/j.heliyon.2024.e39662.
[18] S. Jiang, Z. Gui, Y. Shi, K. Zhou, B. Yuan, C. Bao, S. Lo, Y. Hu, Bismuth subcarbonate nanoplates for thermal stability, fire retardancy and smoke suppression applications in polymers: a new strategy, Polym. Degrad. Stab. 107 (2014) 1–9, https://doi.org/10.1016/j.polymdegradstab. 2014.04.027.
[19] M. Bar, R. Alagirusamy, A. Das, Flame retardant polymer composites, Fibers Polym. 16 (2015) 705–717, https://doi.org/10.1007/s12221-015-0705-6.
[20] Y. Hou, Z. Xu, F. Chu, Z. Gui, L. Song, Y. Hu, W. Hu, A review on metal-organic hybrids as flame retardants for enhancing fire safety of polymer composites, Compos. B Eng. 221 (2021), https://doi.org/10.1016/j.compositesb.2021.109014.
[21] M.J. Mochane, T.H. Mokhothu, T.C. Mokhena, Synthesis, mechanical, and flammability properties of metal hydroxide reinforced polymer composites: a review, Polym. Eng. Sci. 62 (2022) 44–65, https://doi.org/10.1002/pen.25847.
[22] A. Kausar, Flame retardant potential of clay nanoparticles, in: Clay Nanoparticles: Properties and Applications, Elsevier, 2020, pp. 169–184, https://doi.org/10.1016/B978-0-12-816783-0.00007-4.
[23] S. Wendels, T. Chavez, M. Bonnet, K.A. Salmeia, S. Gaan, Recent developments in organophosphorus flame retardants containing P-C bond and their applications, Materials 10 (2017), https://doi.org/10.3390/ma10070784.
[24] J.Z. Liang, Tensile and flexural properties of polypropylene composites filled with highly effective flame retardant magnesium hydroxide, Polym. Test. 60 (2017) 110–116, https://doi.org/10.1016/j.polymertesting.2017.03.014.
[25] X. Qian, L. Song, Y. Bihe, B. Yu, Y. Shi, Y. Hu, R.K.K. Yuen, Organic/inorganic flame retardants containing phosphorus, nitrogen and silicon: preparation and their performance on the flame retardancy of epoxy resins as a novel intumescent flame retardant system, Mater. Chem. Phys. 143 (2014) 1243–1252, https://doi.org/10.1016/j.matchemphys.2013.11.029.
[26] X.H. Shi, Q.Y. Liu, X.L. Li, S.Y. Yang, D.Y. Wang, Simultaneously improving the fire safety and mechanical properties of epoxy resin with iron phosphonated grafted polyethylenimine, Polym. Degrad. Stab. 206 (2022), https://doi.org/10.1016/J.POLYMDEGRADSTAB. 2022.110173.
[27] G.W. Yun, J.H. Lee, S.H. Kim, Flame retardant and mechanical properties of expandable graphite/polyurethane foam composites containing iron phosphonate dopamine-coated cellulose, Polym. Compos. 41 (2020), https://doi.org/10.1002/pc.25578.
[28] R.A. Mensah, V. Shanmugam, S. Narayanan, J.S. Renner, K. Babu, R.E. Neisiany, M. Försth, G. Sas, O. Das, A Review of Sustainable and Environment-friendly Flame Retardants Used in Plastics, 2022, https://doi.org/10.1016/j.polymertesting.2022.107511.
[29] J.A. Andresen, A. Grundmann, K. Bester, Organophosphorus flame retardants and plasticisers in surface waters, Sci. Total Environ. 332 (2004) 155–166, https://doi.org/10.1016/j.scitotenv.2004.04.021.
[30] K.E. Decsov, B. Ötvös, T.T.T. Nguyen, K. Bocz, The effect of cellulose fibre length on the efficiency of an intumescent flame retardant system in poly(lactic acid), Fire 6 (2023), https://doi.org/10.3390/fire6030097.
[31] L. Rajeshkumar, P.S. Kumar, P. Boonyasopon, S.M. Rangappa, S. Siengchin, Flame retardance behaviour and degradation of plant-based natural fiber composites – a comprehensive review, Constr. Build. Mater. 432 (2024), https://doi.org/10.1016/j.conbuildmat.2024.136552.
[32] L. Shumao, R. Jie, Y. Hua, Y. Tao, Y. Weizhong, Influence of ammonium polyphosphate on the flame retardancy andmechanical properties of ramie fiber-reinforced poly(lactic acid) biocomposites, Polym. Int. 59 (2010) 242–248, https://doi.org/10.1002/pi.2715.
[33] X.H. Shi, X.L. Li, Y.M. Li, Z. Li, D.Y. Wang, Flame-retardant strategy and mechanism of fiber reinforced polymeric composite: a review, Compos. B Eng. 233 (2022), https://doi.org/10.1016/j.compositesb.2022.109663.
[34] J. Jiang, Y. Cheng, Y. Liu, Q. Wang, Y. He, B. Wang, Intergrowth charring for flame-retardant glass fabric-reinforced epoxy resin composites, J. Mater. Chem. A Mater. 3 (2015), https://doi.org/10.1039/c4ta06486k.
[35] W. Chen, P. Liu, Y. Liu, Q. Wang, Interfacial carbonation for efficient flame retardance of glass fiber-reinforced polyamide 6, Polym. Chem. 6 (2015) 4409–4414, https://doi.org/10.1039/c5py00280j.
[36] Y. Jiang, J. Pei, Y. Zheng, Y. Jing Miao, B. Zhong Duan, L. Fang Huang, Gallic acid: a potential anti-cancer agent, Chin. J. Integr. Med. 28 (2022) 661–671, https://doi.org/10.1007/s11655-021-3345-2.
[37] K.N. Raymond, E.A. Dertz, S.S. Kim, Enterobactin: an archetype for microbial iron transport, Proc. Natl. Acad. Sci. USA 100 (2003) 3584–3588, https://doi.org/10.1073/PNAS.0630018100.
[38] Q. Kong, Y. Sun, C. Zhang, H. Guan, J. Zhang, D.Y. Wang, F. Zhang, Ultrathin iron phenyl phosphonate nanosheets with appropriate thermal stability for improving fire safety in epoxy, Compos. Sci. Technol. 182 (2019), https://doi.org/10.1016/j.compscitech.2019.107748.
[39] W. Liu, L. Nie, L. Luo, J. Yue, L. Gan, J. Lu, J. Huang, C. Liu, Enhanced dispersibility and uniform distribution of iron phosphonate to intensify its synergistic effect on polypropylene-based intumescent flame-retardant system, J. Appl. Polym. Sci. 137 (2020), https://doi.org/10.1002/app.49552.
[40] N. Song, Y. Suo, F. Rong, K. Wang, Y. Guo, Z. Chen, Y. Yu, T. Chen, J. Jiang, Construction of an organic iron phosphate/graphite carbon nitride hybrid system for improved fire safety of epoxy resin, Mater. Today Sustain. 26 (2024), https://doi.org/10.1016/j.mtsust.2024.100789.
[41] L. Zhang, Z. Li, Y.T. Pan, A.P. Yáñez, S. Hu, X.Q. Zhang, R. Wang, D.Y. Wang, Polydopamine induced natural fiber surface functionalization: a way towards flame retardancy of flax/poly(lactic acid) biocomposites, Compos. B Eng. 154 (2018) 56–63, https://doi.org/10.1016/j.compositesb.2018.07.037.
[42] A. Pantaleoni, F. Sarasini, P. Russo, J. Passaro, L. Giorgini, I. Bavasso, M. L. Santarelli, E. Petrucci, F. Valentini, M.P. Bracciale, A. Marrocchi, Facile and Bioinspired Approach From Gallic Acid for the Synthesis of Biobased Flame Retardant Coatings of Basalt Fibers, 2024, https://doi.org/10.1021/acsomega.3c10129.
[43] E. Lasseuguette, Grafting Onto Microfibrils of Native Cellulose, 2008, https://doi.org/10.1007/s10570-008-9200-1.
[44] B. Fathi, M. Harirforoush, M. Foruzanmehr, S. Saıd Elkoun, M. Robert, Effect of TEMPO oxidation of flax fibers on the grafting efficiency of silane coupling agents, J. Mater. Sci. 52 (n.d.). https://doi.org/10.1007/s10853-017-1224-1.
[45] Y. Wen, Z. Yuan, J. Qu, C. Wang, A. Wang, Evaluation of ultraviolet light and hydrogen peroxide enhanced ozone oxidation treatment for the production of cellulose nanofibrils, ACS Sustain. Chem. Eng. 8 (2020) 2688–2697, https://doi.org/10.1021/acssuschemeng.9b06028.
[46] M. Mołoń, D. Szlachcikowska, K. Stępień, P. Kielar, S. Galiniak, Two faces of TEMPO (2,2,6,6-tetramethylpiperidinyl-1-oxyl) – an antioxidant or a toxin? Biochim. Biophys. Acta, Mol. Cell Res. 1870 (2023) https://doi.org/10.1016/j.bbamcr.2022.119412.
[47] L. Zhang, C. Meng, J. Fu, J. Lou, X. Zhang, W. Gao, X. Fan, Effect of ozone treatment on the chemical and mechanical properties of flax fibers, Ind. Crop. Prod. 189 (2022), https://doi.org/10.1016/j.indcrop.2022.115694.
[48] L. Yan, N. Chouw, K. Jayaraman, Flax fibre and its composites - a review, Compos. B Eng. 56 (2014) 296–317, https://doi.org/10.1016/j.compositesb.2013.08.014.
[49] S. Devarajan, M. Muthuchamy, A. Muthukumar, G.D. Giri, Development of oxidized cellulose fabrics for hemostat applications, Mater. Lett. 308 (2022), https://doi.org/10.1016/j.matlet.2021.131160.
[50] V. Titok, V. Leontiev, S. Yurenkova, T. Nikitinskaya, T. Barannikova, L. Khotyleva, Infrared spectroscopy of fiber flax, J. Nat. Fibers 7 (2010) 61–69, https://doi.org/10.1080/15440470903579275.
[51] M.C. Seghini, F. Touchard, L. Chocinski-arnault, V. Placet, C. François, L. Plasseraud, M.P. Bracciale, J. Tirill, F. Sarasini, Environmentally friendly surface modification carbon dioxide, Molecules 25 (2020) 1–16.
[52] Y. Rosen, H. Mamane, Y. Gerchman, Short ozonation of lignocellulosic waste as energetically favorable pretreatment, Bioenergy Res. 12 (2019) 292–301, https://doi.org/10.1007/s12155-019-9962-3.
[53] G.J.M. van der Kerk, J.H. Verbeek, J.C.F. Cleton, Preparation of esters of gallic acid with higher primary alcohols, Recl. Trav. Chim. Pays-Bas 70 (1951) 277–284, https://doi.org/10.1002/RECL.19510700310.
[54] D. Prat, A. Wells, J. Hayler, H. Sneddon, C.R. Mcelroy, S. Abou-Shehada, P. J. Dunn, CHEM21 selection guide of classical-and less classical-solvents †, Green Chem. 18 (2015) 288, https://doi.org/10.1039/c5gc01008j.
[55] D. Ho, J. Lee, S. Park, Y. Park, K. Cho, F. Campana, D. Lanari, A. Facchetti, S. Y. Seo, C. Kim, A. Marrocchi, L. Vaccaro, Green solvents for organic thin-film transistor processing, J. Mater. Chem. C Mater. 8 (2020) 5786–5794, https://doi.org/10.1039/D0TC00512F.
[56] C. Tsioptsias, I. Tsivintzelis, Insights on thermodynamic thermal properties and infrared spectroscopic band assignments of gallic acid, J. Pharm. Biomed. Anal. 221 (2022) 115065, https://doi.org/10.1016/j.jpba.2022.115065.
[57] I. Mohammed-Ziegler, F. Billes, Vibrational spectroscopic calculations on pyrogallol and gallic acid, J. Mol. Struct. (THEOCHEM) 618 (2002) 259–265, https://doi.org/10.1016/S0166-1280(02)00547-X.
[58] K.N. Raymond, B.E. Allred, A.K. Sia, Coordination Chemistry of Microbial Iron Transport, 2015, https://doi.org/10.1021/acs.accounts.5b00301.
[59] P. Sánchez, N. Gálvez, E. Colacio, E. Miñones, J.M. Domínguez-Vera, Catechol releases iron(III) from ferritin by direct chelation without iron(II) Production, (n.d.). https://doi.org/10.1039/b416669h.
[60] P. Bhanja, K. Ghosh, S. Safikul Islam, A.K. Patra, S. Manirul Islam, A. Bhaumik, New Hybrid Iron Phosphonate Material as an Efficient Catalyst for the Synthesis of Adipic Acid in Air and Water, 2016, https://doi.org/10.1021/acssuschemeng.6b02023.
[61] Z. Aytac, S.I. Kusku, E. Durgun, T. Uyar, Encapsulation of gallic acid/cyclodextrin inclusion complex in electrospun polylactic acid nanofibers: release behavior and antioxidant activity of gallic acid, Mater. Sci. Eng. C 63 (2016) 231–239, https://doi.org/10.1016/J.MSEC.2016.02.063.
[62] V. Kocman, G.M. Di Mauro, G. Veglia, A. Ramamoorthy, Use of paramagnetic systems to speed-up NMR data acquisition and for structural and dynamic studies, Solid State Nucl. Magn. Reson. 102 (2019) 36–46, https://doi.org/10.1016/j.ssnmr.2019.07.002.
[63] X. Xia, X. Shi, W. Liu, H. Zhao, H. Li, Y. Zhang, Effect of flax fiber content on polylactic acid (PLA) crystallization in PLA/flax fiber composites, Iran. Polym. J. (Engl. Ed.) 26 (2017) 693–702, https://doi.org/10.1007/s13726-017-0554-9.
[64] M.R.N. Fazita, K. Jayaraman, D. Bhattacharyya, M.S. Hossain, M.K.M. Haafiz, H. P.S. Abdul Khalil, Disposal options of bamboo fabric-reinforced poly(lactic) acid

composites for sustainable packaging: biodegradability and recyclability, Polymers (Basel) 7 (2015) 1476–1496, https://doi.org/10.3390/polym7081465.
[65] B. Schartel, C.A. Wilkie, G. Camino, Recommendations on the scientific approach to polymer flame retardancy: part 2 - concepts, J. Fire Sci. 35 (2017) 3–20, https://doi.org/10.1177/0734904116675370.
[66] P. Carty, S. White, Iron Based Flame Retarding/Smoke Suppressing Compounds for Thermoplastic Polymers &, 1994.
[67] Y. Peng, M. Niu, R. Qin, B. Xue, M. Shao, Study on flame retardancy and smoke suppression of PET by the synergy between Fe2O3 and new phosphorus-containing silicone flame retardant, High Perform. Polym. 32 (2020) 871–882, https://doi.org/10.1177/0954008320914365.
[68] X. Chen, L. Liu, C. Jiao, Influence of iron oxide brown on smoke-suppression properties and combustion behavior of intumescent flame-retardant epoxy composites, Adv. Polym. Technol. 34 (2015), https://doi.org/10.1002/adv.21516.
[69] A. Marcilla, A. Gómez-Siurana, S. Menargues, Qualitative study of the evolution of the composition of the gas evolved in the thermal and HY-catalytic oxidative degradation of EVA copolymers, Thermochim. Acta 438 (2005) 155–163, https://doi.org/10.1016/j.tca.2005.07.015.
[70] B.N. Jang, C.A. Wilkie, The thermal degradation of bisphenol a polycarbonate in air, Thermochim. Acta 426 (2005) 73–84, https://doi.org/10.1016/j.tca.2004.07.023.
[71] C. Wang, H. Bi, Q. Lin, X. Jiang, C. Jiang, Co-pyrolysis of sewage sludge and rice husk by TG–FTIR–MS: pyrolysis behavior, kinetics, and condensable/non-condensable gases characteristics, renew, Energy 160 (2020) 1048–1066, https://doi.org/10.1016/j.renene.2020.07.046.
[72] I.C. McNeill, H.A. Leiper, Degradation studies of some polyesters and polycarbonates-2. Polylactide: degradation under isothermal conditions, thermal degradation mechanism and photolysis of the polymer, Polym. Degrad. Stab. 11 (1985) 309–326, https://doi.org/10.1016/0141-3910(85)90035-7.
[73] M.K. Amin, J. Boateng, Surface functionalization of PLGA nanoparticles for potential oral vaccine delivery targeting intestinal immune cells, Colloids Surf. B: Biointerfaces 222 (2023) 113121, https://doi.org/10.1016/j.colsurfb.2022.113121.
[74] H. Zou, C. Yi, L. Wang, H. Liu, W. Xu, Thermal degradation of poly(lactic acid) measured by thermogravimetry coupled to Fourier transform infrared spectroscopy, J. Therm. Anal. Calorim. 97 (2009) 929–935, https://doi.org/10.1007/s10973-009-0121-5.
[75] W. Xie, Z. Gao, W.P. Pan, D. Hunter, A. Singh, R. Vaia, Thermal degradation chemistry of alkyl quaternary ammonium montmorillonite, Chem. Mater. 13 (2001) 2979–2990, https://doi.org/10.1021/cm010305s.
[76] G.A. Wang, W.M. Cheng, Y.L. Tu, C.C. Wang, C.Y. Chen, Characterizations of a new flame-retardant polymer, Polym. Degrad. Stab. 91 (2006) 3344–3353, https://doi.org/10.1016/j.polymdegradstab. 2006.06.001.
[77] Y. Cao, Z. Chen, M. Boukhir, B. Dong, J. Zhang, S. Gu, S. Zhang, Insight into the pyrolysis of bamboo flour, polylactic acid and their composite: pyrolysis behavior, kinetic triplets, and thermodynamic parameters based on Fraser-Suzuki deconvolution procedure, Bioresour. Technol. 391 (2024) 129932, https://doi.org/10.1016/j.biortech.2023.129932.
[78] M. Liang, H. Pan, Y. Zhu, H. Zhu, M. Su, Y. Xie, Y. Zheng, X. Jiang, R. Li, J. Zhang, Co-pyrolysis behavior of polylactic acid and biomass from heated tobacco products, Biomass Convers. Biorefinery (2023), https://doi.org/10.1007/s13399-023-04575-1.
[79] B. Lin, J. Zhou, Q. Qin, X. Song, Z. Luo, Thermal behavior and gas evolution characteristics during co-pyrolysis of lignocellulosic biomass and coal: a TG-FTIR investigation, J. Anal. Appl. Pyrolysis 144 (2019) 104718, https://doi.org/10.1016/j.jaap.2019.104718.
[80] S.K. Majhi, S.K. Nayak, S. Mohanty, L. Unnikrishnan, Mechanical and fracture behavior of banana fiber reinforced polylactic acid biocomposites, Int. J. Plast. Technol. 14 (2010) 57–75, https://doi.org/10.1007/s12588-010-0010-6.
[81] S. Li, C. Wang, X. Zhuang, Y. Hu, F. Chu, Renewable resource-based composites of acorn powder and polylactide bio-plastic: preparation and properties evaluation, J. Polym. Environ. 19 (2011) 301–311, https://doi.org/10.1007/s10924-010-0280-2.
[82] B.D. Lazic, S.D. Janjic, T. Rijavec, M.M. Kostic, Effect of chemical treatments on the chemical composition and properties of flax fibers, J. Serb. Chem. Soc. 82 (2017) 83–97, https://doi.org/10.2298/JSC160707106L.
[83] S. Rongpipi, D. Ye, E.D. Gomez, E.W. Gomez, Progress and opportunities in the characterization of cellulose – an important regulator of cell wall growth and mechanics, Front. Plant Sci. 9 (2019) 1–28, https://doi.org/10.3389/fpls.2018.01894.
[84] K.S. Salem, N.K. Kasera, M.A. Rahman, H. Jameel, Y. Habibi, S.J. Eichhorn, A. D. French, L. Pal, L.A. Lucia, Comparison and assessment of methods for cellulose crystallinity determination, Chem. Soc. Rev. 52 (2023) 6417–6446, https://doi.org/10.1039/d2cs00569g.
[85] M.A. Sawpan, K.L. Pickering, A. Fernyhough, Effect of various chemical treatments on the fibre structure and tensile properties of industrial hemp fibres, Compos. Part A Appl. Sci. Manuf. 42 (2011) 888–895, https://doi.org/10.1016/j.compositesa.2011.03.008.
[86] T. He, M. Liu, X. Tian, Effect of Active Hydroxylamine Intermediates on Improving Cellulose Protection and Mass Transfer in Ozone Bleaching of Low-consistency Pulp, 2019, https://doi.org/10.1016/j.indcrop.2019.05.054.
[87] A. Arbelaiz, G. Cantero, B. Fernández, I. Mondragon, P. Gañán, J.M. Kenny, Flax fiber surface modifications: effects on fiber physico mechanical and flax/polypropylene interface properties, Polym. Compos. 26 (2005) 324–332, https://doi.org/10.1002/pc.20097.
[88] J.K.W. Chang, X. Duret, V. Berberi, H. Zahedi-Niaki, J.M. Lavoie, Two-step thermochemical cellulose hydrolysis with partial neutralization for glucose production, Front. Chem. 6 (2018) 1–11, https://doi.org/10.3389/fchem.2018.00117.
[89] P. Gañán, I. Mondragon, Surface modification of fique fibers. Effects on their physico-mechanical properties, Polym. Compos. 23 (2002) 383–394, https://doi.org/10.1002/pc.10440.
[90] N.S. Çetin, P. Tingaut, N. Özmen, N. Henry, D. Harper, M. Dadmun, G. Sèbe, Acetylation of cellulose nanowhiskers with vinyl acetate under moderate conditions, Macromol. Biosci. 9 (2009) 997–1003, https://doi.org/10.1002/mabi.200900073.
[91] Y. Nishiyama, J. Sugiyama, H. Chanzy, P. Langan, Crystal Structure and Hydrogen Bonding System in Cellulose I r From Synchrotron X-ray and Neutron Fiber Diffraction, 2003, https://doi.org/10.1021/ja037055w.
[92] M. Wada, L. Heux, Y. Nishiyama, P. Langan, X-ray Crystallographic, Scanning Microprobe X-ray Diffraction, and Cross-polarized/magic Angle Spinning 13 C NMR Studies of the Structure of Cellulose III II, (n.d.). https://doi.org/10.1021/bm8010227.
[93] A.D. French, Idealized Powder Diffraction Patterns for Cellulose Polymorphs, (n.d.). https://doi.org/10.1007/s10570-013-0030-4.
[94] A. Altomare, C. Cuocci, C. Giacovazzo, A. Moliterni, R. Rizzi, N. Corriero, A. Falcicchio, EXPO2013: a kit of tools for phasing crystal structures from powder data, J. Appl. Crystallogr. 46 (2013) 1231–1235, https://doi.org/10.1107/S0021889813013113.
[95] R. Zhang, T. Miyoshi, P. Sun, NMR Methods for Characterization of Synthetic and Natural Polymers, Royal Society of Chemistry, 2019, https://doi.org/10.1039/9781788016483.
[96] R.S. Dassanayake, N. Dissanayake, J.S. Fierro, N. Abidi, E.L. Quitevis, K. Boggavarappu, V.D. Thalangamaarachchige, Characterization of Cellulose Nanocrystals by Current Spectroscopic Techniques, (n.d.). https://doi.org/10.1080/05704928.2021.1951283.
[97] L. Grunin, M. Ivanova, V. Schiraya, T. Grunina, Time-domain NMR techniques in cellulose structure analysis, Appl. Magn. Reson. 54 (2023) 929–955, https://doi.org/10.1007/S00723-023-01600-4/METRICS.
[98] A.P. More, Flax fiber–based polymer composites: a review, Adv. Compos. Hybrid Mater. 5 (2022) 1–20, https://doi.org/10.1007/s42114-021-00246-9.
[99] A.K. M.D.G. Chandel, F.A. Antunes, P.V. de Arruda, T.S. Milessi, S.S. da Silva, Felipe de Almeida, Dilute acid hydrolysis of agro-residues for the depolymerization of hemicellulose: state-of-the-art, in: D-Xylitol: Fermentative Production, Application and Commercialization, 2012, pp. 36–91, https://doi.org/10.1007/978-3-642-31887-0.
[100] A.N. Round, N.M. Rigby, A.J. MacDougall, V.J. Morris, A new view of pectin structure revealed by acid hydrolysis and atomic force microscopy, Carbohydr. Res. 345 (2010) 487–497, https://doi.org/10.1016/j.carres.2009.12.019.
[101] M.M. Kabir, H. Wang, K.T. Lau, F. Cardona, Chemical treatments on plant-based natural fibre reinforced polymer composites: an overview, Compos. B Eng. 43 (2012) 2883–2892, https://doi.org/10.1016/j.compositesb.2012.04.053.
[102] A. Lefeuvre, A. Bourmaud, C. Morvan, C. Baley, Elementary flax fibre tensile properties: correlation between stress-strain behaviour and fibre composition, Ind. Crop. Prod. 52 (2014) 762–769, https://doi.org/10.1016/j.indcrop.2013.11.043.
[103] A. Bourmaud, C. Morvan, A. Bouali, V. Placet, P. Perré, C. Baley, Relationships between micro-fibrillar angle, mechanical properties and biochemical composition of flax fibers, Ind. Crop. Prod. 44 (2013) 343–351, https://doi.org/10.1016/j.indcrop.2012.11.031.
[104] M.C. Seghini, F. Touchard, F. Sarasini, L. Chocinski-Arnault, J. Tirillò, M. P. Bracciale, M. Zvonek, V. Cech, Effects of oxygen and tetravinylsilane plasma treatments on mechanical and interfacial properties of flax yarns in thermoset matrix composites, Cellulose 27 (2020) 511–530, https://doi.org/10.1007/s10570-019-02785-3.
[105] E. Richely, A. Bourmaud, V. Placet, S. Guessasma, J. Beaugrand, A critical review of the ultrastructure, mechanics and modelling of flax fibres and their defects, Prog. Mater. Sci. 124 (2022) 100851, https://doi.org/10.1016/j.pmatsci.2021.100851.
[106] J. Beaugrand, S. Guessasma, J.E. Maigret, Damage mechanisms in defected natural fibers, Sci. Rep. 7 (2017) 1–7, https://doi.org/10.1038/s41598-017-14514-6.
[107] M. Hughes, Defects in natural fibres: their origin, characteristics and implications for natural fibre-reinforced composites, J. Mater. Sci. 47 (2012) 599–609, https://doi.org/10.1007/s10853-011-6025-3.